AGU100 ADVANCING EARTH AND SPACE SCIENCE

JGR

Journal of Geophysical Research: Biogeosciences

RESEARCH ARTICLE

10.1002/2017JG004207

Temporal Coupling of Subsurface and Surface Soil CO_2 Fluxes: Insights From a Nonsteady State Model and Cross-Wavelet Coherence Analysis

Kimberly E. Samuels-Crow[1], Edmund Ryan[2], Elise Pendall[3], and Kiona Ogle[1,4,5]

[1]School of Informatics, Computing, and Cyber Systems, Northern Arizona University, Flagstaff, AZ, USA, [2]Lancaster Environment Centre, Lancaster University, Lancaster, UK, [3]Hawkesbury Institute for the Environment, Western Sydney University, Penrith, New South Wales, Australia, [4]Department of Biological Sciences, Northern Arizona University, Flagstaff, AZ, USA, [5]Center for Ecosystem Science and Society, Northern Arizona University, Flagstaff, AZ, USA

Key Points:

- Soil respiration is a good proxy for concurrent subsurface CO_2 production in coarse-textured, dry soil with shallow roots and microbes
- Soil texture exerts the largest control on the temporal coherence between subsurface and surface soil CO_2 fluxes
- Lag times between subsurface and surface CO_2 fluxes increase when soil is wet and/or subsurface biota are concentrated deeper in the soil

Supporting Information:

- Supporting Information S1

Correspondence to:
K. E. Samuels-Crow,
kimberly.samuels@nau.edu

Citation:
Samuels-Crow, K. E., Ryan, E., Pendall, E., & Ogle, K. (2018). Temporal coupling of subsurface and surface soil CO_2 fluxes: Insights from a nonsteady state model and cross-wavelet coherence analysis. *Journal of Geophysical Research: Biogeosciences*, *123*, 1406–1424. https://doi.org/10.1002/2017JG004207

Received 2 OCT 2017
Accepted 26 MAR 2018
Accepted article online 30 MAR 2018
Published online 27 APR 2018

Abstract Inferences about subsurface CO_2 fluxes often rely on surface soil respiration (R_{soil}) estimates because directly measuring subsurface microbial and root respiration (collectively, CO_2 production, S_{Total}) is difficult. To evaluate how well R_{soil} serves as a proxy for S_{Total}, we applied the nonsteady state DEconvolution of Temporally varying Ecosystem Carbon componenTs model (0.01-m vertical resolution), using 6-hourly data from a Wyoming grassland, in six simulations that cross three soil types (clay, sandy loam, and sandy) with two depth distributions of subsurface biota. We used cross-wavelet coherence analysis to examine temporal coherence (localized linear correlation) and offsets (lags) between S_{Total} and R_{soil} and fluxes and drivers (e.g., soil temperature and moisture). Cross-wavelet coherence revealed higher coherence between fluxes and drivers than linear regressions between concurrent variables. Soil texture and moisture exerted the strongest controls over coherence between CO_2 fluxes. Coherence between CO_2 fluxes in all soil types was strong at short (~1 day) and long periods (>8 days), but soil type controlled lags, and rainfall events decoupled the fluxes at periods of 1–8 days for several days in sandy soil, up to 1 week in sandy loam, and for a month or more in clay soil. Concentrating root and microbial biomass nearer the surface decreased lags in all soil types and increased coherence up to 10% in clay soil. The assumption of high temporal coherence between R_{soil} and S_{Total} is likely valid in dry, sandy soil, but may lead to underestimates of short-term S_{Total} in semiarid grasslands with fine-grained and/or wet soil.

Plain Language Summary Soil CO_2, which is produced underground by roots and microbes, is a major part of the global carbon cycle. There are large uncertainties over how soil CO_2 will change as global temperatures and atmospheric CO_2 rise. One source of uncertainty is how quickly soil CO_2 moves from the sites where it is produced underground to the surface where it is released to the atmosphere. In this paper, we use a numerical model to test the common assumption that CO_2 produced underground is released immediately to the atmosphere. We found that this assumption is valid when soil is coarse and dry, but there are delays between subsurface CO_2 production and release to the atmosphere when the soil has a fine texture and/or is wet.

1. Introduction

Soil respiration (R_{soil}) represents a major component of the global carbon cycle (e.g., Bond-Lamberty & Thomson, 2010; Cox et al., 2000; Raich & Schlesinger, 1992; Rey, 2015; Roland et al., 2015; Schlesinger & Andrews, 2000; Stoy et al., 2007), but there are large uncertainties in how this flux of CO_2 to the atmosphere will respond and feedback to climate change (e.g., Doetterl et al., 2015; Tang & Riley, 2014). Many ecosystem models predict that increased global temperatures will lead to an increased flux of soil CO_2 to the atmosphere, suggesting that, globally, soil is likely to be a net source of CO_2 as temperatures rise (Crowther et al., 2016; Koven et al., 2011). Though there is a positive correlation between R_{soil} rates and mean annual temperature across a diverse range of ecosystems (e.g., Raich & Schlesinger, 1992), ecosystem-scale and terrestrial biosphere models can give widely varying R_{soil} estimates (Tian et al., 2015). These varying estimates of R_{soil} may be attributed to oversimplifications of modeled soil CO_2 production and efflux processes (e.g., Bond-Lamberty & Thomson, 2010; Luo et al., 2015; Todd-Brown et al., 2013).

A typical simplifying assumption in field and modeling studies is that subsurface CO_2 produced by roots (S_R) and microbes (S_M) is instantly released as R_{soil} (Baldocchi et al., 2006; Jassal et al., 2004; Maier &

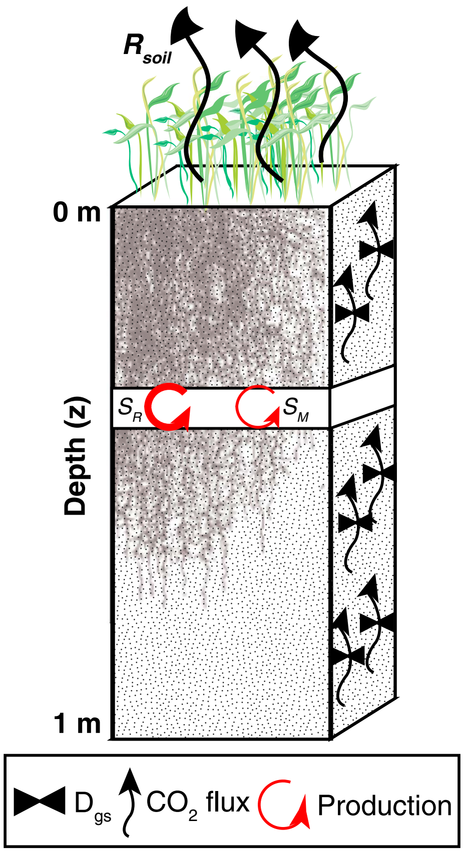

Figure 1. Conceptual model of subsurface CO_2 fluxes described by the DEconvolution of Temporally varying Ecosystem Carbon componenT model. CO_2 concentration at time *t* and depth *z* is a function of biotic (root + microbial) respiration or CO_2 production at that depth (red arrows) and diffusion in and out of that layer (black arrows; Ryan et al., 2018).

Schack-Kirchner, 2014; Pingintha et al., 2010; Vargas et al., 2010), despite empirical evidence for hysteresis between subsurface and surface soil CO_2 fluxes (Baldocchi et al., 2006; Kim et al., 2017; Tang & Baldocchi, 2005; Vargas et al., 2010, 2011; Zhang et al., 2015). Estimating the differences between CO_2 production rates in the soil (e.g., $S_{Total} = S_R + S_M$) versus the CO_2 flux rate from the soil surface to the atmosphere (i.e., R_{soil}) is difficult, mostly due to practical limitations in estimating diffusivity, a key step in converting direct measurements of CO_2 concentrations to fluxes (Maier & Schack-Kirchner, 2014; Risk et al., 2008).

Furthermore, ecosystem-scale studies typically rely on R_{soil} measured at the surface to infer complicated and difficult to measure subsurface root/rhizosphere respiration and/or rates of microbial decomposition of soil organic matter (e.g., Ryan & Law, 2005). For example, such approaches may (1) use steady state models of surface soil CO_2 efflux (R_{soil}) to infer subsurface CO_2 production rates (Del Grosso et al., 2005; Sierra, 2012; Vargas et al., 2010; Zobitz et al., 2008) and/or (2) rely on ^{13}C or ^{14}C measured in surface-respired CO_2 (i.e., isofluxes) to partition subsurface root/rhizosphere and microbial contributions to R_{soil} (Carbone et al., 2008; Kuzyakov, 2006; Pendall et al., 2003; Takahashi et al., 2008). These approaches essentially assume that there is no delay between subsurface CO_2 production and surface measured R_{soil}. In reality, subsurface CO_2 transport processes, which are a function of CO_2 concentration at each depth coupled with soil physical factors that influence both diffusivity and effective path lengths, can lead to temporal lags between subsurface and surface CO_2 fluxes and between CO_2 fluxes and environmental drivers such as T_{soil} and soil water content (SWC; e.g., Vargas et al., 2010; Zhang et al., 2015).

Physical-based models can provide insights into the robustness of the aforementioned simplifying assumptions (Baldocchi et al., 2006; Lee et al., 2004; Ryan et al., 2018; Šimůnek et al., 2012; Tang et al., 2003; Vargas et al., 2010) and should be able to capture temporal lags. Such models should consider the biophysical processes underlying CO_2 production, transport, and efflux, because R_{soil} is a complicated function of both subsurface biological activity (microbial respiration [S_M] and root respiration [S_R]) and CO_2 transport through the soil column (e.g., Stoy et al., 2007; Figure 1). Therefore, variables that influence S_M and S_R, such as soil temperature (T_{soil}) and SWC, affect the total amount of CO_2 in the soil column at any given time. Further, the subsurface distribution of roots and microbes can influence diffusivity by creating preferential pathways to the surface (e.g., via macropores or root channels (Angers & Caron, 1998; Devitt & Smith, 2002; Ragab & Cooper, 1993)) and controlling the effective path length for diffusion, from the depth of CO_2 production to the surface where soil CO_2 is emitted to the atmosphere. Finally, physical factors that control CO_2 diffusivity (e.g., soil bulk density, T_{soil}, and SWC) influence the rate at which CO_2 diffuses through the soil column (Moldrup et al., 2001).

Understanding the factors that affect the temporal relationship between R_{soil} and S_{Total} is particularly important in grasslands, which comprise approximately 32% of terrestrial land cover (Oertel et al., 2016). Temperate grasslands play a major role in the carbon cycle and typically serve as carbon sinks that sequester CO_2 in their dense root biomass and soil organic matter (Carrillo et al., 2014; Frank & Dugas, 2001; Oertel et al., 2016). In North America, the native mixed-grass prairie is an extensive temperate grassland that currently serves as a net carbon sink, but it is being increasingly stressed due to grazing and other land use and climate factors (e.g., Zelikova et al., 2014). Changes in temperature, precipitation patterns, and atmospheric CO_2 have the potential to affect the dense root network of this ecosystem, which will likely change seasonal CO_2 fluxes and the temporal relationship between R_{soil} and S_{Total}. These changes influence carbon cycle feedbacks to climate change (Carrillo et al., 2014; Frank & Dugas, 2001; Pendall et al., 2013), underscoring the importance of evaluating assumptions about the relationship between subsurface production and R_{soil}.

Our objective is to evaluate the assumption that CO_2 fluxes measured at the surface (i.e., R_{soil}) are a valid proxy for understanding subsurface CO_2 production by roots/rhizosphere and microbes. Further, we aim to understand how environmental conditions related to subsurface CO_2 production and transport affect the validity of this assumption. We evaluate this assumption by combining a biophysical-based model of soil CO_2 production and transport with time series analysis techniques that provide quantitative insight into the temporal coupling of subsurface and surface CO_2 fluxes. We apply these simulations in the context of a mixed-grass prairie in Wyoming, United States. In doing so, we specifically address the following questions: (1) How do R_{soil} and total subsurface CO_2 production rates ($S_{Total} = S_R + S_M$) vary over subdaily to seasonal time scales in a semiarid grassland? (2) How does soil texture influence the temporal coherence (i.e., the local linear correlation between two time series) and time lags between R_{soil} and S_{Total}? Finally, how do (3) biological (e.g., depth distribution of roots and microbes) factors and (4) physical properties of the soil column (e.g., SWC and T_{soil}) affect the temporal relationship between each CO_2 flux variable (i.e., R_{soil} or S_{Total})? To address these questions, we used the nonsteady state DEconvolution of Temporally varying Ecosystem Carbon componenTs (DETECT) model (Ryan et al., 2018) to calculate both surface R_{soil} and subsurface CO_2 production rates (i.e., S_M and S_R) at subdaily (6 hourly) time steps and fine (0.01 m) depth resolution, and we subsequently applied cross-wavelet coherence (CWC) analysis to examine temporal coherence and offsets (lags) between S_{Total} and R_{soil}.

2. Methods

To evaluate the influence of subsurface CO_2 production and diffusivity through the soil column on the temporal relationship between S_{Total} and R_{soil}, we simulated CO_2 fluxes using the DETECT model. Our goal was to evaluate these relationships under relatively realistic conditions. Thus, DETECT was parameterized based on the well-studied Prairie Heating and CO_2 Enrichment (PHACE) study in Wyoming, United States, (Bachman et al., 2010; Pendall et al., 2013; Zelikova et al., 2015) and run with driving data representative of the PHACE site. We then applied a CWC analysis to the model output to evaluate variability in the temporal relationship between S_{Total} and R_{soil} and between these CO_2 fluxes and environmental driving variables at subdaily to monthly time scales over the course of a single growing season. The DETECT model (Ryan et al., 2018) and CWC techniques (Grinsted et al., 2004; Labat, 2005, 2010; Torrence & Compo, 1998; Vargas et al., 2010) are described in detail elsewhere, but we summarize important aspects in sections 2.2 and 2.3.

2.1. Field Site for Model Parameterization

The PHACE site is situated at an elevation of 1,930 m in a mixed-grass prairie dominated by two C_3 grasses, western wheatgrass (*Pascopyrum smithii* (Rydb.) A. Löve) and needle-and-thread grass (*Hesperostipa comata* Trin and Rupr), and one C_4 grass, blue grama (*Bouteloua gracilis* (H.B.K.) Lag; Bachman et al., 2010). Soil at the site is characterized in the Ascalon series as a fine-loamy, mixed mesic Aridic Argiustoll with no biological crusts (Bachman et al., 2010). This semiarid site (mean annual precipitation = 384 mm) experiences cold winters (mean January temperature = −2.5°C) and moderately warm growing seasons (mean July temperature = 17.5°C; Morgan et al., 2011).

The PHACE experiment involved an incomplete factorial manipulation of temperature, soil water (via supplemental watering), and atmospheric CO_2 concentration. The treatment combinations were applied to 30 instrumented plots (six treatment levels and five replicate plots per treatment level). The CO_2 manipulations involved two levels: ambient (385 ppmv) or elevated (600 ppmv) CO_2 conditions, which were combined with one of two temperature levels (no warming or 1.5°C [3°C] warming in day [night]). The ambient CO_2 and nonwarmed treatments were also combined with one of three irrigation levels (i.e., none, "shallow," and "deep"; Dijkstra et al., 2010). For the purposes of this study, we used data from the ambient and elevated CO_2 plots with ambient temperature and no supplemental watering to inform parameter values in DETECT, including the depth distribution of root and microbial biomass carbon. We did not utilize or discuss data and experimental results from the other treatment combinations. The DETECT model was previously parameterized using these data with the goal of specifying values representative of this mixed-grass prairie site (see Ryan et al. (2018) for details on the parameterization methods and parameter values uses).

2.2. Numerical Simulations

2.2.1. Model Description

DETECT is a nonsteady state, physical-based model of soil CO_2 production and transport that calculates CO_2 concentrations, C (z,t), at each predefined depth (z) and time (t) interval. Underlying DETECT is a partial differential equation (PDE, equation (1)) that describes how CO_2 varies with z and t as a function of physical (i.e., diffusivity, D_{gs} (Moldrup et al., 2001)) and biological (i.e., source term, $S(z,t)$ processes). Here $S(z,t)$ is total CO_2 production rate at depth z and time t associated with microbial decomposition of soil organic matter, $S_M(z,t)$, and root respiration, $S_R(z,t)$, such that $S(z,t) = S_M(z,t) + S_R(z,t)$. For the purposes of our simulation experiments, we assumed that CO_2 production and efflux took place along an idealized vertical soil column and that advection due to bulk air transport and reactions of dissolved CO_2 (Fang & Moncrieff, 1999; Rey, 2015; Roland et al., 2015) were negligible. This allowed us to isolate potential factors that could uncouple surface and subsurface fluxes, in the absence of other confounding processes.

The PDE model that forms the basis of DETECT follows Fang and Moncrieff (1999), as modified by Ryan et al. (2018), and is given by

$$\frac{\partial C(z,t)}{\partial t} = \frac{\partial}{\partial z}\left(D_{gs}(z,t)\frac{\partial C(z,t)}{\partial z}\right) + S(z,t). \tag{1}$$

where C (z,t) is CO_2 concentration (mg CO_2/m^3 soil) at depth z and time t. The soil CO_2 diffusivity submodel for $D_{gs}(z,t)$ (m^2/s) is a function of atmospheric pressure (P), soil physical properties (e.g., total soil porosity, derived from bulk and particle density, air-filled porosity at a soil water potential of −10 kPa, and the pore size distribution), T_{soil}, and SWC at each z and t (Moldrup et al., 1999, 2004). Although the diffusivity submodel does not account for plant-induced changes to physical properties of the soil (e.g., Angers & Caron, 1998; Devitt & Smith, 2002; Ragab & Cooper, 1993) or for phase and air-filled volume changes associated with aqueous chemical reactions, it provides idealized insights into movement of CO_2 from the subsurface to the atmosphere. The treatment of phase and volume changes is consistent with established methods, which are based on the assumption that CO_2 in gas and aqueous phase equilibrate almost instantaneously without driving up the concentration of gaseous CO_2 in a smaller pore volume and that excluding the concentration of aqueous CO_2 does not significantly influence diffusion calculations (e.g., Fang & Moncrieff, 1999). See Ryan et al. (2018) for details.

We solved the PDE in equation (1) numerically via a forward Euler discretization for the time derivative and a centered-difference method for the depth derivative (Haberman, 1998). In doing so, we assumed an initial condition of $C(z, t = 0) = C_0(z)$, coupled with atmospheric CO_2 concentration (C_{atm}, equivalent to 356 ppm) as the upper boundary condition, $C(z = 0, t)$, and a zero-flux lower boundary condition at z = 100 cm (i.e., $\frac{\partial C(z=100,t)}{\partial z} = 0$; Haberman, 1998). The initial depth profile, $C_0(z)$, was informed by field data on observed soil CO_2 concentrations, as described in Ryan et al. (2018). Note that Δt represents the time interval at which model outputs are stored, but the numerical time step at which the PDE is solved is normally substantially smaller than Δt to ensure numerical stability. We conducted simulation tests and determined that a time interval (Δt) of 6 hr and a depth increment (Δz) of 0.01 m provided an accurate, stable, and computationally efficient solution to the PDE, and increasing the spatial and temporal resolution (e.g., Δt = 1 hr and Δz = 0.005 m) did not significantly change the numerical results. The model achieved numerical stability after 44 time steps (i.e., days 1 to 11), so we considered the first 11 days as a model "spin-up" and removed these from our analysis. See Ryan et al. (2018) for a more detailed overview of the numerical solution approach.

Each component of the subsurface CO_2 production or source term (i.e., $S_M(z,t)$ and $S_R(z,t)$) was determined separately based on previously published models that have been tested in a number of settings (Davidson et al., 2012, 2006; Lloyd & Taylor, 1994; Luo & Zhou, 2010; Ryan et al., 2015; Todd-Brown et al., 2012). The microbial contribution, $S_M(z,t)$, was calculated based on a modified Dual-Arrhenius Michaelis-Menton (DAMM) model (Davidson et al., 2012; Lloyd & Taylor, 1994; Luo & Zhou, 2010; Ryan et al., 2015; Todd-Brown et al., 2012). The DAMM model describes microbial decomposition rates (CO_2 production) based on Michaelis-Menton dynamics for enzymatic reactions, which are, in turn, controlled by T_{soil}, carbon substrate availability, and microbial carbon use efficiency (Davidson et al., 2012; Lloyd & Taylor, 1994). Root respiration, $S_R(z,t)$, is described by a function that describes the effect of both temperature (akin to an energy-of-activation model, (Lloyd & Taylor, 1994)) and SWC, as informed by studies of soil and ecosystem

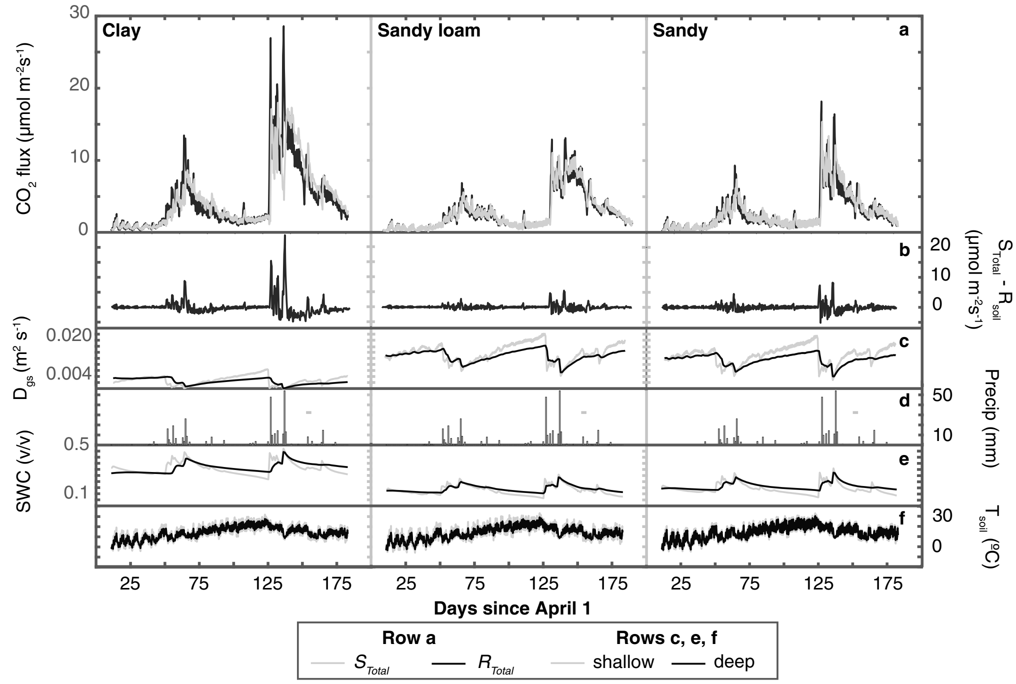

Figure 2. Time series of DEconvolution of Temporally varying Ecosystem Carbon componenT model predictions of (a) total CO_2 fluxes (S_{Total}, gray curve, and R_{soil}, black curve), (b) the difference between subsurface (S_{Total}) and surface (R_{soil}) CO_2 fluxes at each time step, (c) soil CO_2 diffusivity (D_{gs}) averaged across shallow (0.05 to 0.15 m, gray curve) and deep (0.35 to 0.45 m, black curve) intervals. These DEconvolution of Temporally varying Ecosystem Carbon componenT predictions are driven by environmental data, including (d) daily precipitation, (e) shallow (0.05 to 0.15 m, gray curve) and deep (0.35 to 0.45 m, black curve) soil water content (SWC), and (f) shallow (0.03 m, gray curve) and deep (0.05 m, black curve) soil temperature (T_{soil}). While D_{gs}, SWC, and T_{soil} values were available for each 0.01 m down to 1 m, we only show example output or data for the depths and depth intervals measured at the Wyoming Prairie Heating and CO_2 Enrichment site. Results are shown for each soil texture (columns) scenario applied in combination with the depth distribution of roots and microbes scenario, which corresponds to predicted fluxes under ambient CO_2 (C_{atm} = 385 ppmv) conditions.

respiration (Cable et al., 2013; Luo & Zhou, 2010; Ryan et al., 2015). DETECT expands on the DAMM and Lloyd and Taylor models for S_M and the S_R model by applying the calculations to each soil depth (z) and by allowing both current and past (antecedent) T_{soil} and SWC to modify both S_M and S_R (Ryan et al., 2015). See Ryan et al. (2018) for details on the S_M and S_R submodels.

We calculated total subsurface production rates and total surface soil respiration rates as follows. First, we calculated the total CO_2 production rate in the entire soil column at time t, $S(t)$ (mg C · cm^3 · hr^1) by summing the depth-specific production rates (equation (2)):

$$S(t) = \sum_{z=0.01\ \text{m}}^{z=1\ \text{m}} \left(S_M(z,t) + S_R(z,t)\right). \tag{2}$$

We then calculated S_{Total} by converting $S(t)$ to flux units (µmol CO_2 · m^2 · s), using a conversion factor of 6.3117×10^{-5} µmol CO_2 · m^2 · s/mg C · cm^3 · hr. The total flux of CO_2 from the soil surface to the atmosphere (R_{soil}, µmol CO_2 · m^2 · s) was computed as follows:

$$R_{soil}(t) = \frac{D_{gs}(z = 0.01\ \text{m}, t)}{\Delta z}\left(C(z = 0.01\ \text{m}, t) - C_{atm}(t)\right). \tag{3}$$

where D_{gs}(z = 0.01 m, t) and C(z = 0.01 m, t) are the CO_2 diffusivity and concentration, respectively, calculated for the top soil layer (z = 0.01 m), and $C_{atm}(t)$ is the atmospheric CO_2 concentration at time t.

2.2.2. Environmental Driving Data

DETECT requires continuous environmental data as inputs to compute CO_2 production, transport, and efflux, including meteorological data (e.g., air temperature and atmospheric pressure), subsurface soil conditions (e.g., SWC and T_{soil}), and indices of aboveground vegetation activity (e.g., greenness). Again, we drew upon

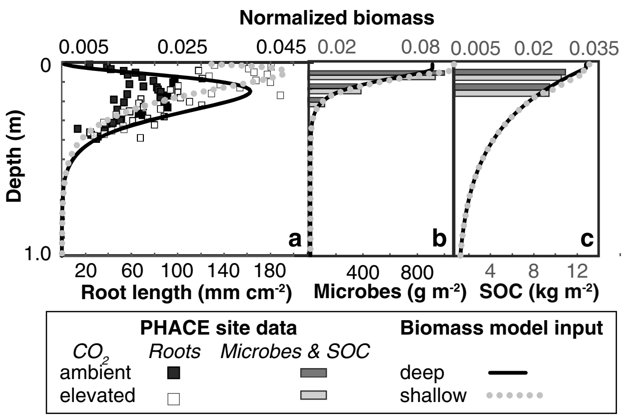

Figure 3. We approximated the root biomass, microbial biomass, and soil organic carbon (SOC) depth distributions based on Prairie Heating and CO_2 Enrichment (PHACE) site data from plots with ambient (C_{atm} = 385 ppmv) and elevated (C_{atm} = 600 ppmv), including data (bottom *x* axes) on (a) root length (squares), measured by minirhizotrons to a depth of 0.4 m, (b) microbial biomass (bars) measured at depths centered on 0.05, 0.10, and 0.15 m, and (c) SOC (bars) measured at depths centered on 0.05 and 0.10 m. Statistical models were fit to these data to extrapolate to 1 m, producing continuous distributions of normalized (top x axes; a) root biomass, (b) microbial biomass, and (c) SOC for the deep (black curve) and shallow (gray dotted curve) biomass distribution scenarios. See text for details.

the wealth of information from the PHACE study to provide realistic inputs to the DETECT model, with the goal of simulating soil CO_2 dynamics representative of a real semiarid grassland ecosystem.

Following Ryan et al. (2018), we used data from an "average climate year," the 2008 growing season (1 April to 30 September), at the PHACE site to drive the DETECT model. The total and daily average precipitation (340 and 1.9 mm, respectively) during the 2008 growing season were within 1 standard deviation of the average seasonal and daily rainfall (total: 279 ± 84 and daily: 1.5 ± 0.46 mm) measured at the site from 2004 to 2013. There were two major precipitation events in 2008, each of which occurred within 1 day of the peak average daily events representative of the "typical" (2004 to 2013) growing season. More than 70% of the 2008 growing season precipitation fell during these two major series of storms, which occurred from days 52 to 68 (23 May to 8 June; ~100 mm of rain) and days 125 to 138 (4 to 17 August; ~165 mm). Long rain-free episodes preceded each multiday precipitation event (Figure 2d). These precipitation patterns influenced the temporal and depth variation of SWC (Figure 2e) and T_{soil} (Figure 2f), which are important inputs to the DETECT model.

With the exception of the meteorological data, field measurements were discontinuous both temporally and spatially, but the model requires inputs scaled to the time and depth interval appropriate for DETECT. We averaged hourly meteorological data to obtain 6-hourly inputs. We used a simple linear interpolation to gap-fill greenness values to the appropriate temporal scale (Ryan et al., 2015). At the PHACE site, SWC was monitored daily at three depth intervals (5–15, 15–25, and 35–45 cm), and T_{soil} was recorded hourly at two depths (3 and 10 cm). We gap-filled and interpolated SWC and T_{soil} to a 6-hourly time step and 0.01-m depth increment to a depth of 1 m using the physical-based soil water model, HYDRUS-1D v4.16.0090 (Ryan et al., 2018; Šimůnek et al., 2012, 2008), driven by site-level soil properties and meteorological data, including precipitation. Although DETECT calculates changes to carbon fluxes at each depth and time, the SWC and T_{soil} results presented here focus on field measurement depths for T_{soil}, and averaged across each field depth interval for SWC since these, or similar, depths are frequently used in field studies. In the results and discussion, we evaluate the influence of "shallow" (T_{soil} = 3 cm; SWC = 5–15 cm) and "deep" (T_{soil} = 10 cm; SWC = 35–45 cm) T_{soil} and SWC. Details are provided in Ryan et al. (2018).

DETECT also requires information about the depth distribution of root and microbial biomass and soil organic carbon (SOC). Again, we used data from the PHACE study to obtain realistic depth distributions of these quantities. We smoothed and extrapolated distributions of subsurface biomass and organic carbon observed in different experimental treatment plots at the PHACE site to evaluate the influence of different root and microbial distributions that develop under varying environmental conditions. We focused our analysis on experimental plots (see section 2.1) with ambient (385 ppmv) and elevated (600 ppmv) CO_2 because preliminary analyses indicated that they exhibited the most distinct differences in the depth distribution of roots, microbes, and SOC. We used root and microbial biomass measurements from the top 0.40 m and extrapolated these distributions to a depth of 1 m along with SOC profiles described by Ryan et al. (2018). To help characterize root distributions, we used minirhizotron data collected to a depth of 0.40 m in 2008 (Carrillo et al., 2014) and fit gamma distribution functions to these measurements separately for the ambient and elevated CO_2 plots. Roots measured at the PHACE site were generally longer under elevated CO_2 conditions and were concentrated in the upper 0.10 m while roots were concentrated at depths of around 0.20 m under ambient CO_2 conditions (Figure 3a).

We used data collected annually from soil cores to characterize the depth distribution of microbial biomass (Figure 3b) and SOC (Figure 3c; Dijkstra et al., 2012). We modeled these distributions as gamma and exponential distribution functions, respectively, to obtain interpolated values to a depth of 1 m. Root (and microbial) distributions were shallower under elevated CO_2 than ambient conditions (Mueller et al., 2018), and we refer to these variable distributions of subsurface biomass as the "shallow" (informed by elevated CO_2 plots in the PHACE experiment) and "deep" (informed by ambient plots in the PHACE experiment) biomass scenarios.

2.2.3. Simulation Experiments

To evaluate the influences of soil texture (question 2), distribution of subsurface biomass (question 3), and environmental factors (question 4) on the temporal relationship between S_{Total} and R_{soil}, we used DETECT to simulate CO_2 fluxes based on three different soil texture scenarios (clay, sandy loam, and sandy) and associated SWC and T_{soil}, crossed with two scenarios for the distribution of roots and microbes (shallow and deep). We based soil properties for the sandy loam scenario (20% clay, 20% silt, and 60% sand) on soil at the PHACE site (Bachman et al., 2010) and varied the proportions of clay and sand relative to this scenario to establish soil properties for the other two scenarios: clay (60% clay, 20% silt, and 20% sand) and sandy (10% clay, 10% silt, and 80% sand). As described in Ryan et al. (2018), these soil texture scenarios, along with site meteorological data, were input to the HYDRUS-1D model to simulate time- and depth-varying input data for SWC and T_{soil} for each soil texture scenario. The simulated SWC and T_{soil} data were combined with the depth-varying root and microbial distributions to drive DETECT, producing 6-hourly outputs of D_{gs}, root, and microbial production (i.e., S_R and S_M), and S_{Total} and R_{soil} (Figure 2a).

In establishing our simulation experiments, we attempted to control for the number of variables that could influence the temporal relationships between R_{soil} and S_{Total} and between these fluxes and their environmental drivers. For this reason, we did not incorporate plant-soil feedbacks into our analysis. While it is possible that changes in root, microbial, or soil carbon could feedback to affect soil physical properties or that soil physical properties could influence the distribution of roots, microbes, or SOC, we chose to independently vary biomass distributions and soil properties in our simulation experiments. This flexibility allowed us to tease apart the effects of each of these factors on the temporal coherence between R_{soil} and S_{Total} and between CO_2 fluxes and their environmental drivers.

2.2.4. Informal Model Validation

We evaluated DETECT's ability to predict reasonable R_{soil} values by comparing R_{soil} output (equation (3)) with measurements of R_{soil} obtained via soil chambers deployed in vegetated PHACE plots exposed to ambient CO_2 and temperature (Ogle et al., 2016). We used R_{soil} values that were measured twice a month in 2008, from 1 April to 30 September, producing a total of 60 measurements across the 5 replicate plots for the ambient CO_2 (control) treatment. CO_2 concentrations measured over time in each chamber were converted to fluxes via linear regression in a Bayesian framework. We matched median values of these flux calculations to the average of 6-hourly DETECT output from the same day.

Although the model was not formally parameterized with data from the PHACE site, the DETECT output was within the 95% credible interval of, and followed the same temporal trends as, R_{soil} calculated from measurements at the PHACE site (Figure S1 in the supporting information). This is consistent with the analysis by Ryan et al. (2018), which showed that chamber measurements of R_{eco} along with observed CO_2 concentrations in the subsurface were consistent with DETECT output. Variability in R_{soil} measurements at the site increased during the two precipitation events, most likely due to nonuniform conditions in soil moisture. Median R_{soil} measurements during the August precipitation event were up to 3 times lower than DETECT estimates during this period. These discrepancies are likely due to variable soil moisture conditions at the site (e.g., variations in infiltration) versus the idealized SWC input to DETECT. Nonetheless, the DETECT output was still contained within the 95% credible interval of the measurements. Further, the coefficient of determination between measured and modeled R_{soil} was 0.77 ($p = 0.000109$), indicating a high level of agreement between modeled and measured R_{soil}.

2.3. CWC Analysis

CWC analysis provided insights into the time scales and conditions when it is appropriate to assume R_{soil}, measured (or modeled) at the surface, is a direct representation of subsurface CO_2 production rates.

2.3.1. Background on CWC Analysis

CWC was developed by geophysicists to evaluate temporal relationships between time series with nonstationary periodicity without imposing user-defined assumptions about frequencies of interest or temporal lags between the data sets (Grinsted et al., 2004; Torrence & Compo, 1998; Vargas et al., 2010). This type of analysis has been critical in identifying subseasonal variations in the temporal relationships between R_{soil}

and its drivers, which are difficult to identify through other time series methods that assume invariant temporal relationships between drivers and responses (Vargas et al., 2010, 2011). In this analysis, each time series is transformed into a wavelet (i.e., a finite form of a wave function) to obtain a continuous time signal. The wavelet transformation is based on a "mother wavelet," which is a complex function that is scaled to capture the range of frequencies represented in the time series of interest. There are several functions available to construct a mother wavelet, each of which has tradeoffs in time and frequency resolution (Vargas et al., 2010). Once the time series is transformed to a wavelet, it is then smoothed and crossed with a wavelet that represents the other time series of interest to evaluate the linear correlation at a range of frequencies. If the correlation is outside the range of edge effects (i.e., "cone of influence") and different from the "red noise" background, it is deemed significant. Equations and details for CWC analysis can be found in Torrence and Compo (1998), Grinsted et al. (2004), Labat (2005, 2010), and Vargas et al. (2010).

Importantly, CWC analysis provides information about both temporal coherence and lags between two time series. Temporal coherence can be thought of as short-term linear correlation in time-frequency space (Grinsted et al., 2004). The degree of coherence is expressed as an R^2 term, which quantifies the coherence between the two signals, and has a formula (equation (4)) that bears some similarity to a correlation coefficient localized in time-frequency space (Grinsted et al., 2004):

$$R^2(s) = \frac{\left|S\left(s^{-1}W_n^{XY}(s)\right)\right|^2}{S\left(s^{-1}\left|W_n^X(s)\right|^2\right)\cdot S\left(s^{-1}\left|W_n^Y(s)\right|^2\right)} \tag{4}$$

W_n^X and W_n^Y are the normalized wavelets for each time series (e.g., X and Y) under consideration, W_n^{XY} is the cross-wavelet transform of the two time series, and s is the circular standard deviation as described in Grinsted et al. (2004). The S functions are smoothing operators specific to the mother wavelet chosen for each analysis (Grinsted et al., 2004; Torrence & Compo, 1998).

CWC analysis also produces phase angle (PA) values, which represent offsets or temporal lags, between the time series, for each time step and period. A PA, which is proportional to a temporal lag, can be thought of as the difference between the points at which each wavelet (time series) passes through the horizontal axis. The conversion of the calculated offset (PA) to an explicit time lag leads to nonunique solutions due to uncertainty in the PA (e.g., a PA of $\pi/2$ radians or 90° appears to be the same as a PA of $(5\pi)/2$ radians or 450° when visualized on a unit circle). Therefore, quantifying time lags based on this approach must be done cautiously. Time lags can, nonetheless, be estimated based on PA by eliminating PA values that yield lags that exceed the period (Grinsted et al., 2004).

2.3.2. Implementation of CWC Analysis

We used CWC analysis to evaluate temporal relationships, at multiple time scales, between total CO_2 fluxes (R_{soil} or S_{Total}) and (1) each other ($Y = R_{soil}$, $X = S_{Total}$), (2) T_{soil} ($Y = R_{soil}$ or S_{Total}, $X = T_{soil}$), and (3) SWC ($Y = R_{soil}$ or S_{Total}, $X =$ SWC). We implemented the CWC analysis using the cross-wavelet and wavelet coherence Matlab toolbox (Griffis et al., 2016; Grinsted et al., 2004) and used a Morlet wavelet as the mother wavelet. The Morlet wavelet is commonly used in geophysical and ecological studies because this complex wave provides a balance between time and frequency localization (Grinsted et al., 2004; Torrence & Compo, 1998; Vargas et al., 2010).

Each DETECT model run produced time series outputs that spanned 183 days at a time step (Δt) of 6 hr for a total of 732 simulated CO_2 fluxes during the growing season. After removing the results from the spin-up period (see section 2.2.1), the results of the CWC analysis are expressed in terms of "periods," which are inversely proportional to the frequency of the time series. A period of 1, therefore, represents a single time step (6 hr), a period of 4 is equivalent to a single day, and a period of 128 is equivalent to a 32-day (approximately monthly) time block. Evaluating coherence at different periods provided insights into the time scales over which R_{soil} measured at the surface was a direct picture of subsurface production and the time scales over which R_{soil} might not have provided information about concurrent subsurface processes. Further, the CWC analysis provided insights into the temporal relationships between environmental drivers (e.g., T_{soil} and SWC) and production and R_{soil}. For each analysis, we explored the influence of soil texture and the distribution of root and microbial biomass carbon on the temporal relationships between the time series of interest. When evaluating the temporal relationship between CO_2 fluxes and T_{soil} or SWC, we focused on the relationship at soil depths or depth intervals for which these variables were measured at the Wyoming PHACE site (see Ryan et al. (2018)), which correspond roughly to typical depths used in many field studies, allowing us to address implications of analyzing field-based, empirical data.

We estimated time lags between the *Y* and *X* variables by calculating the PA (in radians) between the two time series and scaling it by the period: lag = PA × period/(2π) (Grinsted et al., 2004). We chose the smallest PA of all possibilities when estimating temporal lags to gain insights into the changes in the temporal relationship between the CO_2 fluxes at subdaily to monthly periods. To summarize the temporal relationships across the entire growing season, we averaged both R^2 and lag values over time within a given period for each soil texture and biomass distribution scenario.

3. Results

We present results from DETECT model simulations and the associated CWC analysis in the context of our main research questions. We first summarize predicted S_{Total} and R_{soil} variations over subdaily to seasonal time scales (question 1) and link these variations to seasonal precipitation patterns and modeled changes in soil CO_2 diffusivity (D_{gs}), exploring how soil texture (question 2) and the depth distribution of roots and microbes (question 3) influence the temporal coherence and lags between R_{soil} and S_{Total}. We then evaluate the temporal relationship between each soil CO_2 flux variable and physical drivers (SWC and T_{soil}; question 4).

3.1. Seasonal Variation in R_{soil} and S_{Total}

The DETECT model predicted that the total amount of CO_2 produced per square meter in the subsurface over the course of the growing season (sum of S_{Total} over the 183-day period) was within 1% of the total amount of CO_2 emitted from the surface (sum of R_{soil}), regardless of soil texture or the distribution of subsurface biomass carbon. Total seasonal fluxes were predicted to be approximately 1.6 times higher in clay soil than in both sandy loam and sandy soil (Figure S2).

Precipitation was concentrated in two main periods, early season (~days 50–75) and late season (days 125–135). Both S_{Total} and R_{soil} increased during the two multiday precipitation events, with the greatest increase during the second event, regardless of soil texture (Figure 2a). These rain events led to increases in SWC (Figure 2e) that coincided with suppression of diffusivity, D_{gs} (Figure 2e), especially in sandy and sandy loam soils. In the clay soil, SWC remained above 0.25 (i.e., 25% *v*/v) throughout the growing season whereas the sandy and sandy loam soils had lower water holding capacities. Because of its relatively high SWC, the clay soil had D_{gs} values roughly 3 times lower than the sandy and sandy loam soils (Figure 2c). T_{soil} increased to a maximum of ~30°C on day 125 in all soil types and then decreased at the start of the second precipitation event (Figure 2f). The combination of soil moisture and temperature led to similar temporal patterns (but different magnitudes) of S_{total} and R_{soil} in all soil types (Figure 2a). Clay soil had the highest fluxes, up to 29 μmol · m^2 · s, and the difference between S_{total} and R_{soil} was greatest in the clay soil (Figure 2b). These differences were most pronounced when SWC and T_{soil} were highest, contributing to higher production rates in clay soil. These higher production rates coincided with the lowest D_{gs}, increasing the lag times between surface efflux and subsurface production.

3.1.1. Temporal Coherence Between R_{soil} and S_{Total} in the Deep-Biomass (Ambient CO_2) Scenario

R_{soil} and S_{Total} were positively correlated (in phase) at daily to monthly periods in all soil texture scenarios during times with little to no precipitation and relatively dry soil (Figure 4). However, over subdaily to daily periods, there was either no coherence between $R_{\underline{soil}}$ and S_{Total} (blue colors, Figure 4) or there were lags between the two fluxes in all soil types, with S_{Total} consistently leading R_{soil}. Regardless of soil texture, PA at subdaily to daily time scales ranged from 45° to 135° when the soil was dry. The PA range can be interpreted as a temporal lag of 0.5 to 1.5 periods or 3 to 9 hr (0.5 (1.5) period × 6 hr/period = 3 (9) hr). These lags were most apparent in the first 25 days of the simulated growing season, during an extended rain-free episode. During and immediately after precipitation events, there was little to no coherence between the R_{soil} and S_{Total} time series at subdaily to biweekly periods in clay soil (Figure 4a) and daily to weekly periods in sandy loam and sandy soils (Figures 4b and 4c). The deterioration of the temporal coherence at these periods lasted for up to a month in clay soil (Figure 4a), up to a week in sandy loam soil, and 1 or 2 days in sandy soil (Figures 4b and 4c).

The CWC analysis revealed temporal lags between R_{soil} and S_{Total} in soil of all textures during and following the two main precipitation pulses. During the first precipitation event (days 52 to 68, 23 May to 8 June), in all

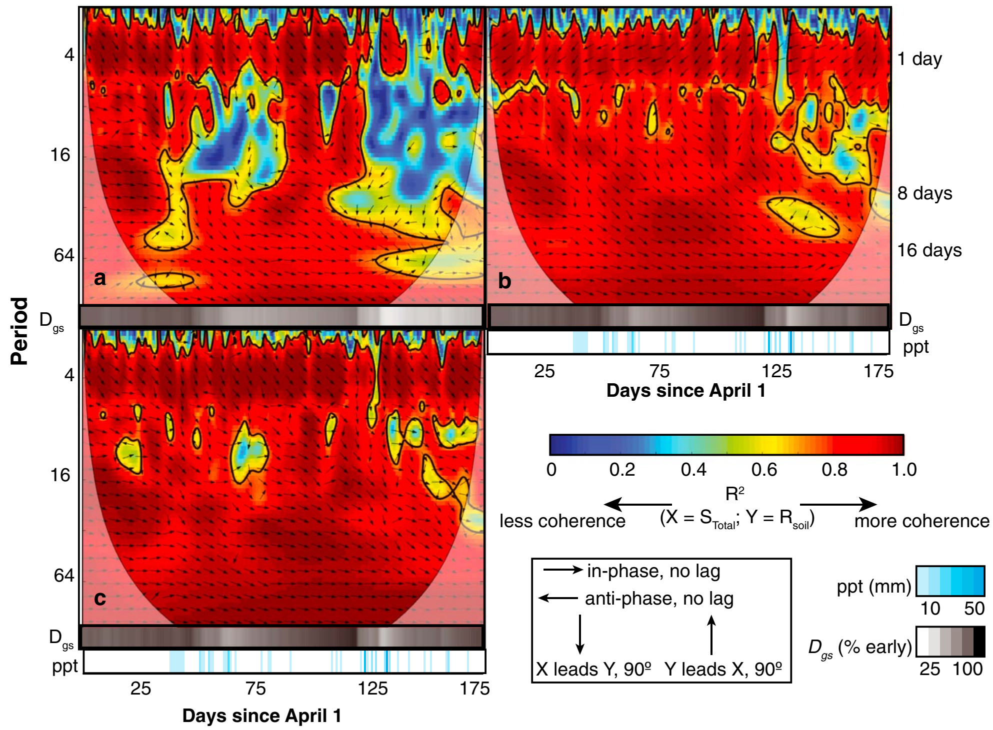

Figure 4. Cross-wavelet coherence plots demonstrate the temporal coherence between modeled soil respiration (R_{soil}; Y) and total subsurface CO_2 production (S_{Total}; X) over the course of the growing season in (a) clay, (b) sandy loam, and (c) sandy soil. Colors are scaled to show coherence (R^2) between the two time series at different periods (Δt = 6 hr, so the time scale is subdaily when period <4 and daily when period = 4). Statistically significant R^2 values are outlined with a heavy black line. Arrows on the cross-wavelet coherence plots indicate the phase angle between the two time series. Phase angle arrows that point to the right indicate that the two time series are in phase (e.g., positively correlated with no lags) while arrows that point to the left are antiphase (e.g., negatively correlated with no lags). Arrows pointing down (up) indicate that the X (Y) time series leads the Y (X) time series by 90° (π/2 radians). The precipitation (ppt) panel (bottom) shows the timing and magnitude of precipitation events over the course of the growing season, while the diffusivity (D_{gs}) gray scale bar (above ppt panel) indicates the CO_2 diffusivity at each time step, averaged over all depth intervals, as a percent of D_{gs} at the start of the growing season, when the soil were relatively dry (high air-filled porosity).

soil types (Figure 4) a temporal lag of at least 6 hr was observed between the time CO_2 was produced within the soil profile and the time it was emitted to the atmosphere. This lag between the two time series was again apparent at the start of the second precipitation event (day 125, 4 August) in the sandy and sandy loam soils, but, in general, there were few lags between R_{soil} and S_{Total} at biweekly to monthly periods in these two soil types (Figures 4b and 4c). In clay soil, there was limited coherence between S_{Total} and R_{soil} at biweekly and shorter time scales during each precipitation episode. When coherence was significant in clay soil during these precipitation episodes, there were temporal lags of at least 48 hr (Figure 4a). This means that during precipitation events, it could take up to 2 days for CO_2 produced in the subsurface to be emitted to the atmosphere in the clay soil scenario (Figure 4a).

The timing of the decreased coherence in clay soil and increased lags in sandy loam and sandy soils corresponds to the timing of suppressed D_{gs} (averaged across all depths) in all soil types (gray bars under each wavelet plot in Figure 4). D_{gs} decreased by approximately 50% in all soil types in the middle of the first multiday precipitation event (around day 60). In clay soil, D_{gs} remained ~16% below pregrowing season values at the start of the second multiday precipitation event (around day 125) while D_{gs} in sandy loam and sandy soil recovered and was approximately 20% higher than early growing season values around day 125 (Figure 2c and gray bars in Figure 4). There was a sharp decrease in D_{gs} in all soil types with the onset of the second precipitation event, but D_{gs} remained approximately 67% below early growing season values in clay soil and recovered to 100% of early growing season values in the coarser sandy loam and sandy soil (Figure 4).

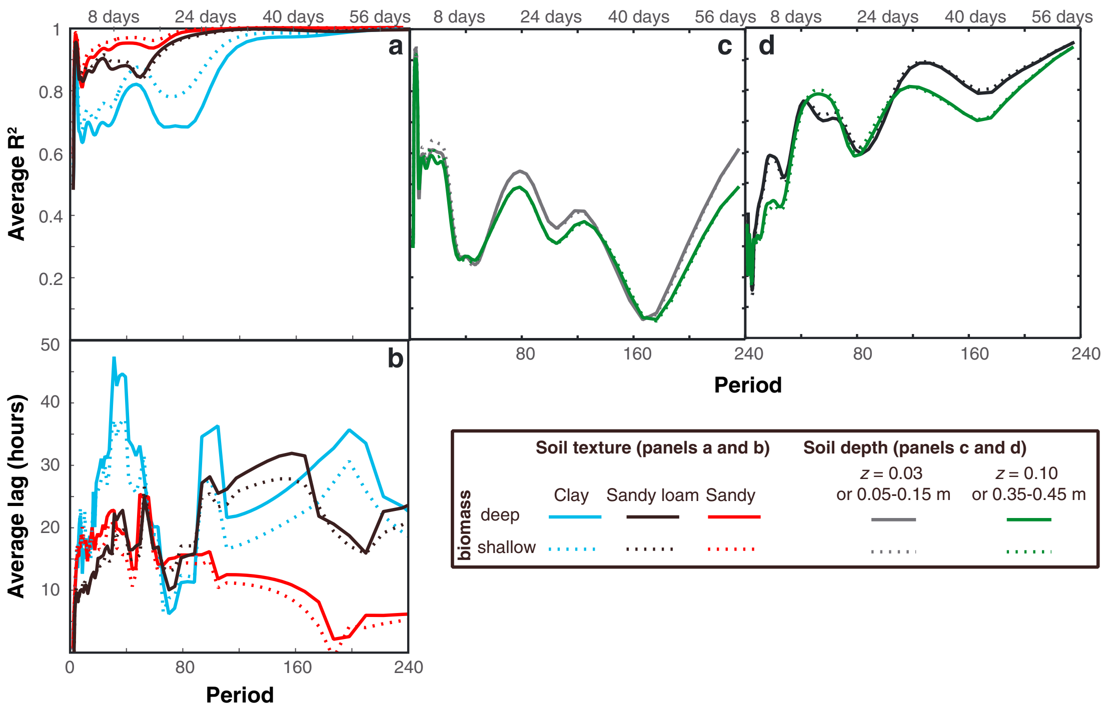

Figure 5. Summaries of the cross-wavelet coherence analysis give (a) the average temporal coherence (R^2) between R_{soil} (Y) and S_{Total} (X) in a given period under the deep versus shallow biomass distribution scenarios (denoted by line type) in the three soil types (denoted by line colors), (b) corresponding average lag time (hr) between R_{soil} and S_{Total}, (c) average R^2 between R_{soil} (Y) and T_{soil} (X) measured at z = 0.03 m (shallow) and z = 0.10 m (deep), and (d) R_{soil} (Y) and soil water content (X) at z = 0.05 to 0.10 m (shallow) and z = 0.35 to 0.45 m (deep).

3.1.2. Effect of Shifting the Distribution of Subsurface Biota to Shallower Soil Layers

Concentrating biomass in the upper 0.1 m of the soil column ("shallow" biomass scenario) had little impact on the overall coherence between R_{soil} and S_{Total}, but it did decrease lag times between these two fluxes relative to the "deep" biomass scenario. The overall coherence between R_{soil} and S_{total} was generally insensitive to the distribution of roots and microbes in the sandy and sandy loam soils, with a difference in average R^2 of less than 0.1 at all periods (Figure 5a). In clay soil, R^2 values were higher by approximately 0.10 in the shallow biomass scenario. In all soil types, time lags between R_{soil} and S_{Total} were shorter in the shallow-biomass scenarios (Figure 5b). Average lag times for a given period decreased by up to 10 hr in clay soil, 5 hr in sandy loam soil, and 2 hr in sandy soil when the biomass was concentrated in the uppermost 0.10 m of the soil column.

3.2. Influence of T_{soil} and SWC

When R_{soil} was related directly to concurrent subsurface environmental drivers (T_{soil} and SWC), correlation coefficients were significantly lower than maximum coherence determined using CWC techniques that take into account lags and a varying temporal structure. For example, when R_{soil} (Y) was regressed on concurrent T_{soil} (X) at 0.03 m or 0.10 m, the coefficient of determination was low ($R^2 \leq 0.10$; Figures 6a and 6b), but regressions of R_{soil} on SWC from 0.05 to 0.15 m or 0.35to 0.45 m produced R^2 values as high as 0.63 (Figures 6c and 6d). However, CWC revealed higher average coherence (R^2 values) between R_{soil} and these environmental drivers (Figures 5c and 5d), due to the ability to account for different time scales and lags.

3.2.1. Temporal Relationships Between CO_2 Fluxes and T_{soil}

CWC analysis indicated that both S_{Total} and R_{soil} (Y variables) were highly coherent with shallow (0.03 m) and deep (0.10 m) T_{soil} (X variable) when the soil was dry, regardless of soil type and the depth distribution of roots and microbes (Figure 7). In general, CO_2 fluxes were coherent with T_{soil} at multiple time scales (1 to 16 days) when the soil was dry. In contrast, CO_2 fluxes and T_{soil} were coherent only at short to intermediate (1 to 4 days) time scales during rainy periods. Coherence between R_{soil} and T_{soil} deteriorated during the second precipitation episode late in the growing season in clay soil.

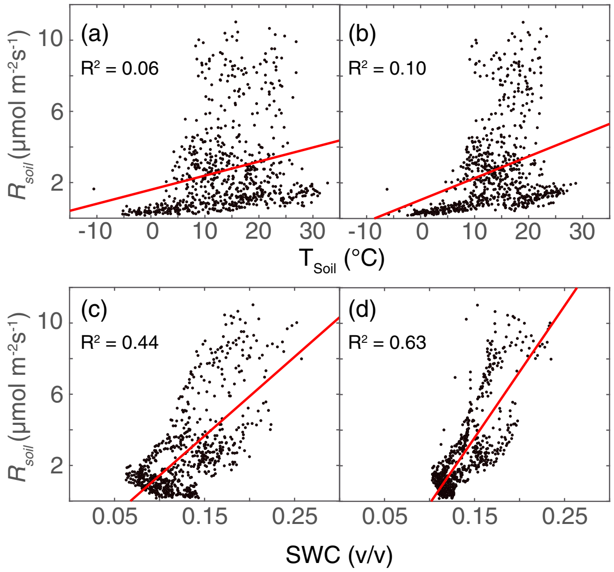

Figure 6. Relationship between predicted R_{soil} and concurrent T_{soil} interpolated from observations measured at (a) $z = 0.03$ m and (b) $z = 0.10$ m; the correlation between R_{soil} and concurrent T_{soil} is much lower than estimated by the cross-wavelet coherence analysis (see Figure 5). Correlations between R_{soil} and concurrent soil water content (SWC) measured at (c) $z = 0.05$ to 0.15 m and (d) $z = 0.35$ to 0.45 m were moderately high and comparable to the cross-wavelet coherence analysis.

Although coherence between R_{soil} or S_{Total} (Y variables) and T_{soil} (X) was generally high during nonrainy times at relatively short and intermediate time scales, regardless of soil type and the distribution of roots and microbes, temporal lags between both R_{soil} or S_{Total} versus T_{soil} varied between soil type. Generally, S_{Total} was highly coherent with both shallow ($z = 0.03$ m; Figure 7a) and deep ($z = 0.10$ m; Figure 7c) T_{soil} at the daily to biweekly time scale. However, lag times between each CO_2 flux and shallow T_{soil} were longer (~3 hr in sandy loam [shown] and 6 hr in clay [not shown] soil). Lag times were generally longer between R_{soil} and T_{soil} in all soil types (Figures 7b and 7d) when compared to the relationship between S_{Total} and T_{soil} (Figure 7).

3.2.2. Temporal Relationships Between CO_2 Fluxes and SWC

R_{soil} and S_{Total} were highly coherent with shallow (0.05 to 0.15 m) and deep (0.35 to 0.45 m) SWC at periods of 4 days or longer during the dry episode between the two multiday precipitation events. Earlier in the growing season, the CO_2 fluxes were only coherent with SWC prior to the onset of the first precipitation episode, and the coherence structure again deteriorated during the second multiday precipitation event. During the two main precipitation episodes, there was high coherence and few lags between each CO_2 flux and SWC at periods of 1–2 weeks and 1 month in sandy loam soil regardless of subsurface biomass distribution. There were few lags between S_{Total} or R_{soil} versus shallow SWC in sandy loam soil (Figures 8a and 8b), but the high coherence between both S_{Total} or R_{soil} versus deep SWC (Figures 8c and 8d)

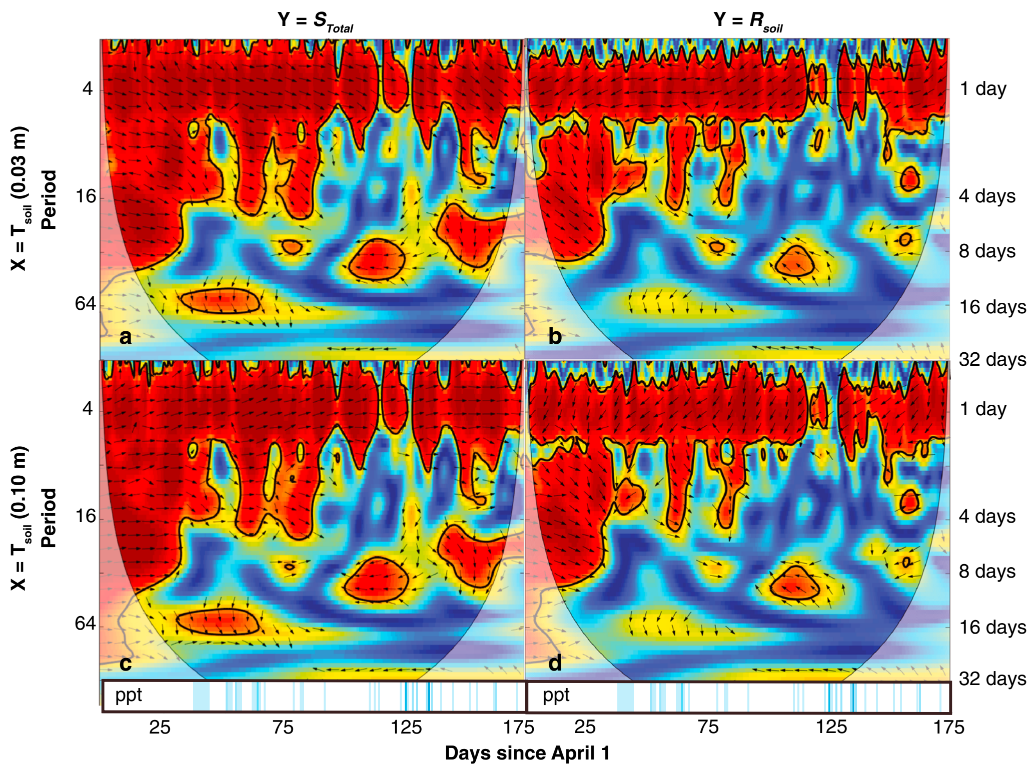

Figure 7. Cross-wavelet coherence plots of subsurface ($Y = S_{Total}$; panels a and c) and surface ($Y = R_{soil}$; panels b and d) CO_2 fluxes with soil temperature ($X = T_{soil}$) at daily to weekly periods. Results are shown for sandy loam soil under the deep-biomass scenario (i.e., ambient CO_2 conditions) but are generally the same, with amplified temporal lags, in clay soil and decreased temporal lags under the shallow-rooted (elevated CO_2 conditions) scenario. The color scales for R^2 and precipitation values and explanation of arrows are the same as in Figure 5.

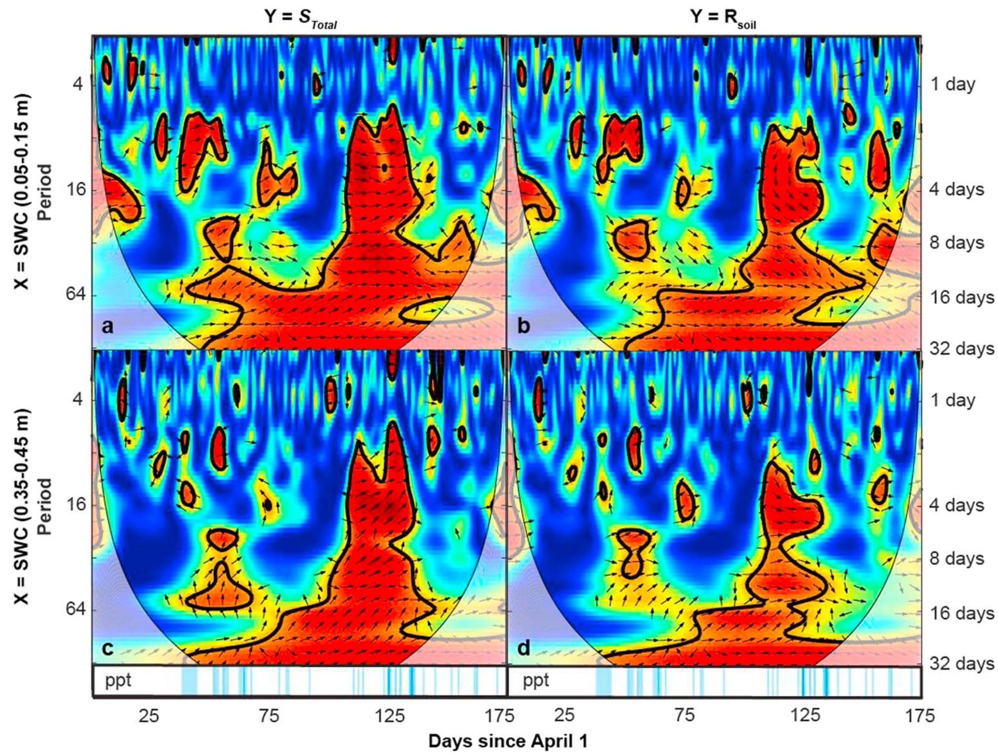

Figure 8. Cross-wavelet coherence plots of subsurface ($Y = S_{Total}$; panels a and c) and surface ($Y = R_{soil}$; panels b and d) CO_2 fluxes with shallow (panels a and b) and deep (panels c and d) soil moisture (X = soil water content [SWC]). Results are shown for sandy loam soil with the deeper biomass (ambient CO_2) scenario but are generally the same, with amplified temporal lags in clay soil and shorter temporal lags in the shallow biomass (elevated CO_2) scenario. The color scales for R^2 and precipitation values and explanation of arrows are the same as in Figure 5.

at periods of 1 week and 1 month was characterized by lags of up to 3 days at the weekly period and up to 2 weeks at the monthly period. In clay soil, there was little coherence between each CO_2 flux and SWC at periods of less than a month.

4. Discussion

The purpose of this study was to evaluate the common and simplifying assumptions that soil respiration (R_{soil}) measured at the soil surface is a reliable proxy for concurrent subsurface CO_2 production by roots and microbes (i.e., S_{Total}) and that R_{soil} can be modeled as a function of concurrently varying soil drivers (e.g., T_{soil} and SWC). Our modeling results indicate that at seasonal time scales, R_{soil} and subsurface CO_2 fluxes are essentially equivalent, at least for the soil textures and root and microbial depth distributions considered here. However, at subdaily to monthly time scales, there are variations in temporal coherence and time lags between R_{soil} and S_{Total} that depend on soil texture, the depth distribution of roots and microbes, and soil environmental drivers (e.g., T_{soil} and SWC) that may invalidate the assumption that R_{soil} provides a snapshot of concurrent subsurface CO_2 production. Soil texture, and the associated SWC and T_{soil} profiles, exerted the strongest control over the temporal coherence and time lags between subsurface and surface CO_2 fluxes, while the depth distribution of root and microbial biomass carbon mainly affected the time lags between the two fluxes.

4.1. Temporal Coherence of R_{soil} and S_{Total}

The two multiday precipitation events increased the magnitude of both S_{Total} and R_{soil}, which is consistent with observations at the site (Figure S1) and elsewhere (Kim et al., 2017), including in other semiarid and arid regions (Deng et al., 2012). R_{soil} at the Wyoming PHACE site also increased following precipitation episodes, but the magnitude of that increase after the second precipitation event was lower than predicted by DETECT.

Previous studies have attributed increased R_{soil} following precipitation events to physical mechanisms (e.g., displacement of CO_2 stored in dry soil pores (Huxman et al., 2004; Kim et al., 2012; Marañón-Jiménez et al., 2011)) or biological mechanisms (e.g., increased microbial metabolism (Kim et al., 2017)). R_{soil} can also decrease following precipitation events, which has also been attributed to physical (e.g., decreased D_{gs} (Davidson et al., 2000; Kim et al., 2012; Rochette et al., 1991; Šimůnek & Suarez, 1993)) and biological processes (e.g., shift from aerobic to anaerobic decomposition (Ball et al., 1999; Davidson et al., 2000; Kim et al., 2012)).

Although the current DETECT model does not explicitly consider physical displacement of soil CO_2 by water nor a shift from aerobic to anaerobic metabolism (expected to be rare in this ecosystem), we can make inferences regarding the causes of increased R_{soil} following precipitation. For example, increases in R_{soil} due to displacement would likely be short-lived, and there is little evidence to suggest that the sustained increase in R_{soil} observed at the PHACE site and predicted by DETECT during rain events can be attributed to physical displacement of CO_2 (Xu & Baldocchi, 2004). Increased SWC does lead to reduced D_{gs} in the model, which would likely lead to decreased R_{soil}, regardless of changes in root and/or microbial CO_2 production. DETECT does allow us to evaluate the contributions of both microbial (S_M) and root (S_R) CO_2 production to the increase in CO_2 fluxes following rain. S_M increased first following precipitation events, followed by increases in both root respiration (S_R) and R_{soil}. For this reason, we attribute the increase in S_{Total} and R_{soil} primarily to increased subsurface biological activity following an influx of moisture.

Although DETECT did not predict decreased R_{soil} during precipitation events, lag times between R_{soil} and subsurface CO_2 production (S_{Total}) increased during the two rainfall events in coarse soil, coherence deteriorated between the two fluxes in fine-grained soil, and S_{Total} consistently exceeded R_{soil} at the start of each multiday precipitation event and on days when total precipitation was relatively high (Figure 2). This implies that precipitation, and the resulting T_{soil} and SWC profiles, decreased CO_2 diffusivity in all soil types (Ryan & Law, 2005), but the effect was strongest in the fine-grained (clay) soil. Soil bulk density and particle size distribution exert a direct control over CO_2 diffusivity because they control pore size distribution, water retention, and air-filled and total porosity at each depth and time (Moldrup et al., 2001; Rey, 2015; Ryan et al., 2018; Sala et al., 1992). Thus, soil texture influenced temporal coherence and time lags between simulated R_{soil} and S_{Total} in a number of ways, with a net result that temporal coherence between the two CO_2 fluxes was highest, and lag times shortest, in coarse soil with little clay (Figure 5). Soil texture also modulated responses to environmental drivers such as precipitation and the resulting T_{soil} and SWC profiles. Since we did not consider aqueous transport and storage mechanisms (e.g., CO_2 dissolution) in the formulation of DETECT, we hypothesize that lags associated with precipitation represent minimum temporal offsets between S_{Total} and R_{soil} since CO_2 dissolution in soil water would increase lag times.

4.2. Time Scales of Influence of T_{soil} and SWC

Studies frequently relate R_{soil} measured at the surface to measurements of T_{soil} and/or SWC made at particular locations (depths) within the soil profile in an effort to understand how variations in these factors affect soil CO_2 efflux (Cable et al., 2008, 2011; Davidson et al., 1998; Lloyd & Taylor, 1994; Sierra, 2012) and feedbacks to atmospheric CO_2 (Davidson & Janssens, 2006; Schlesinger & Andrews, 2000). Production and diffusivity are functions of T_{soil} and SWC, which modify base microbial and root respiration rates (Lloyd & Taylor, 1994; Marañón-Jiménez et al., 2011; Moldrup et al., 2001; Ryan et al., 2018; Wang et al., 2014). Evaluating R_{soil} as a function of concurrent T_{soil} measured at the PHACE site, as might be typical of many data analyses, leads to the appearance that there was no relationship between R_{soil} and T_{soil} (Figures 6a and 6b).

CWC analysis, however, provided a more nuanced perspective of the relationships between these variables, such that R_{soil} is generally coupled to T_{soil} but at varying time scales. This suggests a nonstationary relationship between R_{soil} and T_{soil}, which agrees with empirical observations of hysteresis in the R_{soil} versus T_{soil} relationship (Barron-Gafford et al., 2011; Zhang et al., 2015). DETECT predicted that T_{soil} influenced the movement of CO_2 through the soil column and into the atmosphere with highest coherence at short periods when the soil was warm and dry (Figures 7 and 9). At the start of the growing season, high coherence between the CO_2 fluxes (S_{Total} or R_{soil}) versus T_{soil} occurred at longer periods. This high coherence at the start of the growing season is likely related to higher activation energy, which is explicitly modeled in DETECT (Ryan et al., 2018), when T_{soil} is low. This result is consistent with findings of other studies (e.g., Tang & Riley, 2014).

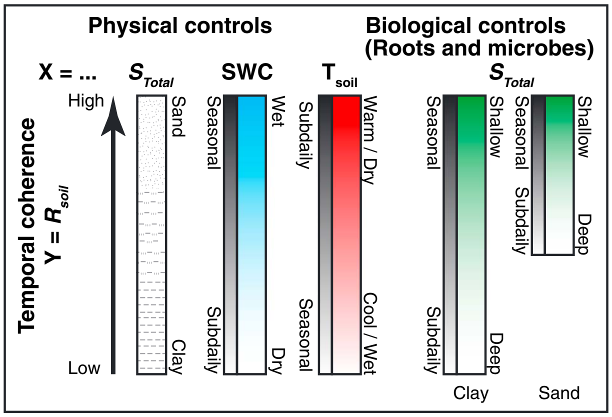

Figure 9. Conceptual summary of the different physical and biological controls on the temporal coherence between surface (R_{soil}) and subsurface (S_{Total}) CO_2 fluxes, which act on different time scales. Soil texture exerted the strongest control over the temporal coherence between R_{soil} and S_{Total}, with the strongest coherence in the more coarse-grained soils. The temporal coherence between R_{soil} and soil water content (SWC) is complicated but is generally high at seasonal time scales during rain-free periods and at weekly or shorter periods during times of precipitation. R_{soil} responds to changes in soil temperature (T_{soil}) at faster time scales when soil is dry. The coherence between R_{soil} and S_{Total} is highest when the subsurface biota (root and microbes) is concentrated in the uppermost 10 cm of the soil column (i.e., under elevated CO_2 conditions), relative to more deeply distributed biota (under ambient CO_2 conditions). Biological factors amplify effects of soil texture rather than exerting a first-order control.

As with T_{soil}, CWC analysis of the relationship between both shallow and deep SWC revealed complicated temporal interactions not evident from simple linear regressions. In contrast to T_{soil}, both R_{soil} and S_{Total} were highly coherent with SWC at long time scales, particularly after the first precipitation episode (Figures 8 and 9). The higher degree of coherence between each CO_2 flux and SWC in deeper soil during the second precipitation episode was consistent with greater infiltration depths associated with the heavier rainfall delivered during this precipitation event (Huxman et al., 2004).

4.3. Effect of Changing the Distribution of Subsurface Biomass

As one might expect, lag times were shorter and temporal coherence between the CO_2 fluxes was higher when root and microbial biomass was concentrated in the uppermost 0.10 m of the soil column (Figure 5). This effect was most dramatic in the clay soil scenario but was also apparent in the coarser soil texture scenarios. Concentrating biomass at shallower depths led to shorter diffusion path lengths, allowing CO_2 produced in the subsurface to reach the surface more quickly (Moldrup et al., 2001), decreasing lag times and increasing temporal coherence.

At the Wyoming PHACE site, elevated atmospheric CO_2 conditions (600 ppmv) favored a plant community with shallower roots compared to ambient CO_2 conditions (385 ppmv; Mueller et al., 2018). As atmospheric CO_2 and temperatures increase globally, grasslands across the region will likely experience changes in plant rooting distributions due to two factors. First, elevated CO_2 may stimulate the local grasses to develop longer, thinner roots to increase exploration for soil water and nutrients (Carrillo et al., 2014). Further, under elevated CO_2, the community composition is shifting to favor species—such as the subdominant C_3 sedge, *Carex duriuscula*—with a greater propensity for root branching (Carrillo et al., 2014; Kropp et al., 2017; Zelikova et al., 2014). Both effects were observed at the Wyoming PHACE site during the experiment, and such shifts in the distribution of roots and associated root litter (substrate for microbes) could impact the utility of using R_{soil} to infer subsurface processes affecting CO_2 fluxes.

4.4. Implications in a Changing Climate

The influence of precipitation and the depth distribution of subsurface biota on the temporal relationships between S_{Total} and R_{soil} suggests that these temporal relationships will likely change as climate changes. In the northern Great Plains, where the Wyoming PHACE site is located, mean annual temperatures have increased at a rate of 2.6°C per century over the course of the instrumental record (Kunkel et al., 2013; Zelikova et al., 2014). Although there is some evidence that this increase in temperature has been accompanied by decreases in precipitation in eastern Wyoming (Ficklin et al., 2013), there are no significant trends in mean annual precipitation across the region. It is, however, likely that growing season precipitation will occur as less frequent, but more intense, storms separated by longer dry periods (Groisman & Knight, 2008; Kunkel et al., 2013; Zelikova et al., 2014). Further, elevated CO_2 led to a shift toward more shallowly distributed root and microbial biomass in this grassland ecosystem during the PHACE experiment. DETECT predicted that this shift to shallower biomass leads to fewer lags between CO_2 production and efflux. Less frequent but more intense storms might lead to increased S_{Total} that is released as R_{soil} with fewer and/or shorter lags as the soil dries between precipitation events. This suggests that the assumption that R_{soil} is a quantitative proxy for S_{Total} in the subsurface may become more valid in semiarid grassland ecosystems as climate changes.

5. Conclusions and Future Directions

The DETECT model provides insights into the validity of assuming R_{soil} measured at the surface is representative of subsurface CO_2 production at the time of measurement. This study indicates that this assumption is generally valid for coarse-grained, dry soil, but it should be cautiously applied in fine-grained and/or wet soil, especially following precipitation events that can dramatically alter soil air-filled porosity and CO_2 diffusivity. The results of this study and others (e.g., Stoy et al., 2007) imply that physical processes can cause lags between CO_2 production and efflux from the soil surface, which can be challenging to distinguish from biologically induced lags, due to, for example, upregulation of root or microbial activity or delayed root or microbial growth. Physical lags are likely more important in finer-textured soils and at higher water contents, particularly at subdaily to daily time scales. These time lags and decoupling between fluxes suggest that R_{soil} measurements do not directly reflect root and microbial activity at the time of measurement, leading to disequilibrium between estimates of S_M, S_R, and R_{soil}, and poor estimates of each subsurface component of R_{soil}. Therefore, any empirical or modeling study that aims to link R_{soil} to subsurface production should consider lags between these CO_2 fluxes particularly in fine-grained and/or wet soil (e.g., depth-averaged SWC $\geq$ 0.2).

The current version of DETECT provides important insights into the primary controls over temporal relationships between subsurface CO_2 production (e.g., S_{Total}) and surface efflux (R_{soil}). Incorporating nondiffusive transport processes into DETECT would improve insights into mechanisms that induce lags between CO_2 production and efflux and between these CO_2 fluxes and their environmental drivers. For example, there is evidence that nondiffusive transport mechanisms (e.g., advection) have a significant impact on the temporal relationships between S_{Total} and R_{soil} and between these fluxes and their environmental drivers, particularly at short time scales (Roland et al., 2015). Further, incorporating an evaluation of carbonate reactions that take place in soil water (e.g., Fang & Moncrieff, 1999) would allow us to explicitly evaluate ephemeral processes that likely affect the presence and magnitude of lags at short time scales, including physical displacement of gaseous CO_2 following rain pulses in semiarid grassland ecosystems. Incorporating these processes may help improve the ability of DETECT to predict the magnitude of R_{soil} following precipitation events and provide better estimates of lags. Further, incorporating these processes would allow us to evaluate the conditions and time scales over which nondiffusive versus diffusive transport processes exert the greatest influences over movement of CO_2 from the subsurface to the atmosphere.

Nonetheless, our results are consistent with a growing body of studies that indicate that temporal lags associated with R_{soil} must be accounted for in carbon cycle models that operate at subseasonal time scales (e.g., Baldocchi et al., 2006; Kim et al., 2017; Stoy et al., 2007; Tang & Baldocchi, 2005; Vargas et al., 2010; Zhang et al., 2015). Further, our current analysis highlights the importance of evaluating how temporal relationships vary over time. This sort of analysis will become more important when examining more detailed mechanistic controls over S_{Total} and R_{soil}.

Acknowledgments

We thank Jack Morgan for supporting soil research at PHACE, and Dan LeCain and David Smith for maintaining the experimental infrastructure. This manuscript is based upon work supported by the U.S. Department of Agriculture Agricultural Research Service Climate Change, Soils and Emissions Program, USDA-CSREES Soil Processes Program (2008-35107-18655), U.S. Department of Energy Office of Science (BER), through the Terrestrial Ecosystem Science program (DE-SC0006973) and the Western Regional Center of the National Institute for Climatic Change Research, and by the National Science Foundation (DEB#1021559). We thank two anonymous reviewers for their assistance in improving the manuscript. The DETECT model, input files, and user manual are available at http://doi.org/10.5281/zenodo.927501. Driving data, parameter values, and model output for the analysis presented here are available in the supporting information and at http://jan.ucc.nau.edu/ogle-lab/zzz_modelDETECT.html in the "JGR example" directory. The Matlab toolbox used for cross wavelet coherence analysis is available at https://www.mathworks.com/matlabcentral/fileexchange/47985-cross-wavelet-and-wavelet-coherence.

References

Angers, D. A., & Caron, J. (1998). Plant-induced changes in soil structure: Processes and feedbacks. *Biogeochemistry*, *42*(1–2), 55–72. https://doi.org/10.1023/A

Bachman, S., Heisler-White, J. L., Pendall, E., Williams, D. G., Morgan, J. A., & Newcomb, J. (2010). Elevated carbon dioxide alters impacts of precipitation pulses on ecosystem photosynthesis and respiration in a semi-arid grassland. *Oecologia*, *162*(3), 791–802. https://doi.org/10.1007/s00442-009-1511-x

Baldocchi, D., Tang, J., & Xu, L. (2006). How switches and lags in biophysical regulators affect spatial-temporal variation of soil respiration in an oak-grass savanna. *Journal of Geophysical Research*, *111*, G02008. https://doi.org/10.1029/2005JG000063

Ball, B. C., Scott, A., & Parker, J. P. (1999). Field N_2O, CO_2, and CH_4 fluxes in relation to tillage, compaction and soil quality in Scotland. *Soil & Tillage Research*, *21*(5), 419–432. https://doi.org/10.1007/s10450-015-9683-7

Barron-Gafford, G. A., Scott, R. L., Jenerette, G. D., & Huxman, T. E. (2011). The relative controls of temperature, soil moisture, and plant functional group on soil CO_2 efflux at diel, seasonal, and annual scales. *Journal of Geophysical Research*, *116*, G01023. https://doi.org/10.1029/2010JG001442

Bond-Lamberty, B., & Thomson, A. (2010). Temperature-associated increases in the global soil respiration record. *Nature*, *464*(7288), 579–582. https://doi.org/10.1038/nature08930

Cable, J. M., Ogle, K., Barron-Gafford, G. A., Bentley, L. P., Cable, W. L., Scott, R. L., et al. (2013). Antecedent conditions influence soil respiration differences in shrub and grass patches. *Ecosystems*, *16*(7), 1230–1247. https://doi.org/10.1007/s10021-013-9679-7

Cable, J. M., Ogle, K., Lucas, R. W., Huxman, T. E., Loik, M. E., Smith, S. D., et al. (2011). The temperature responses of soil respiration in deserts: A seven desert synthesis. *Biogeochemistry*, *103*(1-3), 71–90. https://doi.org/10.1007/s10533-010-9448-z

Cable, J. M., Ogle, K., Williams, D. G., Weltzin, J. F., & Huxman, T. E. (2008). Soil texture drives responses of soil respiration to precipitation pulses in the Sonoran Desert: Implications for climate change. *Ecosystems*, *11*(6), 961–979. https://doi.org/10.1007/s10021-008-9172-x

Carbone, M. S., Winston, G. C., & Trumbore, S. E. (2008). Soil respiration in perennial grass and shrub ecosystems: Linking environmental controls with plant and microbial sources on seasonal and diel timescales. *Journal of Geophysical Research*, *113*, G02022. https://doi.org/10.1029/2007JG000611

Carrillo, Y., Dijkstra, F. A., LeCain, D., Morgan, J. A., Blumenthal, D., Waldron, S., & Pendall, E. (2014). Disentangling root responses to climate change in a semiarid grassland. *Oecologia*, *175*(2), 699–711. https://doi.org/10.1007/s00442-014-2912-z

Cox, P. M., Betts, R. A., Jones, C. D., Spall, S. A., & Totterdell, I. J. (2000). Acceleration of global warming due to carbon-cycle feedbacks in a coupled climate model. *Nature*, *408*(6809), 184–187. https://doi.org/10.1038/35041539

Crowther, T. W., Todd-Brown, K. E. O., Rowe, C. W., Wieder, W. R., Carey, J. C., Machmuller, M. B., et al. (2016). Quantifying global soil carbon losses in response to warming. *Nature*, *540*(7631), 104–108. https://doi.org/10.1038/nature20150

Davidson, E. A., Belk, E., & Boone, R. D. (1998). Soil water content and temperature as independent or confounded factors controlling soil respiration in a temperate mixed hardwood forest. *Global Change Biology*, *4*(2), 217–227. https://doi.org/10.1046/j.1365-2486.1998.00128.x

Davidson, E. A., & Janssens, I. A. (2006). Temperature sensitivity of soil carbon decomposition and feedbacks to climate change. *Nature*, *440*(7081), 165–173. https://doi.org/10.1038/nature04514

Davidson, E. A., Janssens, I. A., & Lou, Y. (2006). On the variability of respiration in terrestrial ecosystems: Moving beyond Q10. *Global Change Biology*, *12*(2), 154–164. https://doi.org/10.1111/j.1365-2486.2005.01065.x

Davidson, E. A., Sudeep, S., Caramori, S. S., & Savage, K. (2012). The Dual Arrhenius and Michaelis–Menten kinetics model for decomposition of soil organic matter at hourly to seasonal time scales. *Global Change Biology*, *18*(1), 371–384. https://doi.org/10.1111/j.1365-2486.2011.02546.x

Davidson, E. A., Verchot, L. V., Cattânio, J. H., Ackerman, I. L., Carvalho, J. E. M., Davidson, E. A., et al. (2000). Effects of soil water content on soil respiration in forests and cattle pastures of eastern Amazonia Source: Biogeochemistry, Vol. 48, No. 1, Controls on Soil Respiration: Implications for Climate Change (Jan., 2000), pp. 53–69 Published by: S. *Biogeochemistry*, *48*(1), 53–69. https://doi.org/10.1023/A:1006204113917

Del Grosso, S. J., Parton, W. J., Mosier, A. R., Holland, E. A., Pendall, E., Schimel, D. S., & Ojima, D. S. (2005). Modeling soil CO_2 emissions from ecosystems. *Biogeochemistry*, *73*(1), 71–91. https://doi.org/10.1007/s10533-004-0898-z

Deng, Q., Hui, D., Zhang, D., Zhou, G., Liu, J., Liu, S., et al. (2012). Effects of precipitation increase on soil respiration: A three-year field experiment in subtropical forests in China. *PLoS One*, *7*(7), e41493–e41499. https://doi.org/10.1371/journal.pone.0041493

Devitt, D. A., & Smith, S. D. (2002). Root channel macropores enhance downward movement of water in a Mojave Desert ecosystem. *Journal of Arid Environments*, *50*(1), 99–108. https://doi.org/10.1006/jare.2001.0853

Dijkstra, F. A., Blumenthal, D., Morgan, J. A., Pendall, E., Carrillo, Y., & Follett, R. F. (2010). Contrasting effects of elevated CO_2 and warming on nitrogen cycling in a semiarid grassland. *The New Phytologist*, *2*, 426–437.

Dijkstra, F. A., Pendall, E., Morgan, J. A., Blumenthal, D. M., Carrillo, Y., Lecain, D. R., et al. (2012). Climate change alters stoichiometry of phosphorus and nitrogen in a semiarid grassland. *New Phytologist*, *196*(3), 807–815. https://doi.org/10.1111/j.1469-8137.2012.04349.x

Doetterl, S., Stevens, A., Six, J., Merckx, R., Van Oost, K., Casanova Pinto, M., et al. (2015). Soil carbon storage controlled by interactions between geochemistry and climate. *Nature Geoscience*, *8*(10), 780–783. https://doi.org/10.1038/ngeo2516

Fang, C., & Moncrieff, J. B. (1999). A model for soil CO_2 production and transport 1. *Agricultural and Forest Meteorology*, *95*(4), 225–236. https://doi.org/10.1016/S0168-1923(99)00036-2

Ficklin, D. L., Stewart, I. T., & Maurer, E. P. (2013). Climate change impacts on streamflow and subbasin-scale hydrology in the Upper Colorado River Basin. *PLoS One*, *8*(8), e71297. https://doi.org/10.1371/journal.pone.0071297

Frank, A. B., & Dugas, W. A. (2001). Carbon dioxide fluxes over a northern, semiarid, mixed-grass prairie. *Agricultural and Forest Meteorology*, *108*(4), 317–326. https://doi.org/10.1016/S0168-1923(01)00238-6

Griffis, T. J., Wood, J. D., Baker, J. M., Lee, X., Xiao, K., Chen, Z., et al. (2016). Investigating the source, transport, and isotope composition of water vapor in the planetary boundary layer. *Atmospheric Chemistry and Physics*, *16*(8), 5139–5157. https://doi.org/10.5194/acp-16-5139-2016

Grinsted, A., Moore, J. C., & Jevrejava, S. (2004). Application of the cross wavelet transform and wavelet coherence to geophysical time series. *Nonlinear Processes in Geophysics*, *11*(5/6), 561–566. https://doi.org/10.1002/etep

Groisman, P. Y., & Knight, R. W. (2008). Prolonged dry episodes over the conterminous United States: New tendencies emerging during the last 40 years. *Journal of Climate*, *21*(9), 1850–1862. https://doi.org/10.1175/2007JCLI2013.1

Haberman, R. (1998). *Elementary applied partial differential equations: With Fourier series and boundary value problems* (3rd ed.). Englewood Cliffs, NJ: Prentice Hall.

Huxman, T. E., Snyder, K. A., Tissue, D., Leffler, A. J., Ogle, K., Pockman, W. T., et al. (2004). Precipitation pulses and carbon fluxes in semiarid and arid ecosystems. *Oecologia*, *141*(2), 254–268. https://doi.org/10.1007/s00442-004-%201682-4

Jassal, R. S., Black, T. A., Drewitt, G. B., Novak, M. D., Gaumont-Guay, D., & Nesic, Z. (2004). A model of the production and transport of CO_2 in soil: Predicting soil CO_2 concentrations and CO_2 efflux from a forest floor. *Agricultural and Forest Meteorology*, *124*(3–4), 219–236. https://doi.org/10.1016/j.agrformet.2004.01.013

Kim, D., Oren, R., Clark, J. S., Palmroth, S., Oishi, A. C., McCarthy, H. R., et al. (2017). Dynamics of soil CO_2 efflux under varying atmospheric CO_2 concentrations reveal dominance of slow processes. *Global Change Biology*, *23*(9), 3501–3512. https://doi.org/10.1111/gcb.13713

Kim, D. G., Vargas, R., Bond-Lamberty, B., & Turetsky, M. R. (2012). Effects of soil rewetting and thawing on soil gas fluxes: A review of current literature and suggestions for future research. *Biogeosciences*, *9*(7), 2459–2483. https://doi.org/10.5194/bg-9-2459-2012

Koven, C. D., Ringeval, B., Friedlingstein, P., Ciais, P., Cadule, P., Khvorostyanov, D., et al. (2011). Permafrost carbon-climate feedbacks accelerate global warming. *Proceedings of the National Academy of Sciences of the United States of America*, *108*(36), 14,769–14,774. https://doi.org/10.1073/pnas.1103910108

Kropp, H., Ogle, K., Vivoni, E. R., & Hultine, K. R. (2017). The sensitivity of evapotranspiration to inter-specific plant neighbor interactions: Implications for models. *Ecosystems*, *20*(7), 1311–1323. https://doi.org/10.1007/s10021-017-0112-5

Kunkel, K. E., Stevens, L. E., Stevens, S. W., & Sun, L. (2013). NOAA technical report NESDIS 142-4 regional climate trends and scenarios for the U. S. National Climate Assessment, (January) (pp. 1–91).

Kuzyakov, Y. (2006). Sources of CO_2 efflux from soil and review of partitioning methods. *Soil Biology and Biochemistry*, *38*(3), 425–448. https://doi.org/10.1016/j.soilbio.2005.08.020

Labat, D. (2005). Recent advances in wavelet analyses: Part 1. A review of concepts. *Journal of Hydrology*, *314*(1–4), 275–288. https://doi.org/10.1016/j.jhydrol.2005.04.003

Labat, D. (2010). Cross wavelet analyses of annual continental freshwater discharge and selected climate indices. *Journal of Hydrology*, *385*(1–4), 269–278. https://doi.org/10.1016/j.jhydrol.2010.02.029

Lee, X., Wu, H. J., Sigler, J., Oishi, C., & Siccama, T. (2004). Rapid and transient response of soil respiration to rain. *Global Change Biology*, *10*(6), 1017–1026. https://doi.org/10.1111/j.1365-2486.2004.00787.x

Lloyd, J., & Taylor, J. A. (1994). On the temperature dependence of soil respiration. *Functional Ecology*, *8*(3), 315–323. https://doi.org/10.2307/2389824

Luo, Y., Keenan, T. F., & Smith, M. (2015). Predictability of the terrestrial carbon cycle. *Global Change Biology*, *21*(5), 1737–1751. https://doi.org/10.1111/gcb.12766

Luo, Y., & Zhou, X. (2010). *Soil respiration and the environment*. San Diego, CA: Academic Press.
Maier, M., & Schack-Kirchner, H. (2014). Using the gradient method to determine soil gas flux: A review. *Agricultural and Forest Meteorology*, *192-193*, 78–95. https://doi.org/10.1016/j.agrformet.2014.03.006
Marañón-Jiménez, S., Castro, J., Kowalski, A. S., Serrano-Ortiz, P., Reverter, B. R., Sánchez-Cañete, E. P., & Zamora, R. (2011). Post-fire soil respiration in relation to burnt wood management in a Mediterranean mountain ecosystem. *Forest Ecology and Management*, *261*(8), 1436–1447. https://doi.org/10.1016/j.foreco.2011.01.030
Moldrup, P., Olesen, T., Komatsu, T., Schjonning, P., & Rolston, D. E. (2001). Tortuosity, diffusivity, and permeability in the soil liquid and gaseous phases. *Soil Science Society of America Journal*, *65*(3), 613–623. https://doi.org/10.2136/sssaj2001.653613x
Moldrup, P., Olesen, T., Yamaguchi, T., Schjonning, P., & Rolston, D. E. (1999). Modeling diffusion and reaction in soils: IX. The Buckingham-Burdine-Campbell equation for gas diffusivity in undisturbed soil. *Soil Science*, *164*(8), 542–551. https://doi.org/10.1097/00010694-199908000-00002
Moldrup, P., Olesen, T., Yoshikawa, S., Komatsu, T., & Rolston, D. E. (2004). Three-porosity model for predicting the gas diffusion coefficient in undisturbed soil. *Soil Science Society of America Journal*, *68*(3), 750–759. https://doi.org/10.2136/sssaj2004.7500
Morgan, J. A., LeCain, D. R., Pendall, E., Blumenthal, D. M., Kimball, B. A., Carrillo, Y., et al. (2011). C4 grasses prosper as carbon dioxide eliminates desiccation in warmed semi-arid grassland. *Nature*, *476*(7359), 202–205. https://doi.org/10.1038/nature%2010274
Mueller, K. E., LeCain, D. R., McCormack, M. L., Pendall, E., Carlson, M., & Blumenthal, D. M. (2018). Root responses to elevated CO_2, warming, and irrigation in a semiarid grassland: Integrating biomass, length, and lifespan in a 5-year field experiment. *Journal of Ecology*. https://doi:10.1111/1365-2745.12993
Oertel, C., Matschullat, J., Zurba, K., Zimmermann, F., & Erasmi, S. (2016). Greenhouse gas emissions from soils—A review. *Chemie der Erde - Geochemistry*, *76*(3), 327–352. https://doi.org/10.1016/j.chemer.2016.04.002
Ogle, K., Ryan, E., Dijkstra, F. A., & Pendall, E. (2016). Quantifying and reducing uncertainties in estimated soil CO_2 fluxes with hierarchical data-model integration. *Journal of Geophysical Research: Biogeosciences*, *121*, 2935–2948. https://doi.org/10.1002/2016JG003385
Pendall, E., Del Grosso, S., King, J. Y., LeCain, D. R., Milchunas, D. G., Morgan, J. A., et al. (2003). Elevated atmospheric CO_2 effects and soil water feedbacks on soil respiration components in a Colorado grassland. *Global Biogeochemical Cycles*, *17*(2), 1046. https://doi.org/10.1029/2001GB001821
Pendall, E., Heisler-White, J. L., Williams, D. G., Dijkstra, F. A., Carrillo, Y., Morgan, J. A., & LeCain, D. R. (2013). Warming reduces carbon losses from grassland exposed to elevated atmospheric carbon dioxide. *PLoS One*, *8*(8), e71921. https://doi.org/10.1371/journal.pone.0071921
Pingintha, N., Leclerc, M. Y., Beasley, J. P. Jr., Zhang, G., & Senthong, C. (2010). Assessment of the soil CO_2 gradient method for soil CO_2 efflux measurements: Comparison of six models in the calculation of the relative gas diffusion coefficient. *Tellus*, *62*(1), 47–58. https://doi.org/10.1111/j.1600-0889.2009.00445.x
Ragab, R., & Cooper, J. D. (1993). Variability of unsaturated zone water transport parameters: Implications for hydrological modelling. 1. In situ measurements. *Journal of Hydrology*, *148*(1–4), 109–131. https://doi.org/10.1016/0022-1694(93)90255-8
Raich, J. W., & Schlesinger, W. H. (1992). The global carbon dioxide flux in soil respiration and its relationship to vegetation and climate. *Tellus B*, *44*(2), 81–99. https://doi.org/10.1034/j.1600-0889.1992.t01-1-00001.x
Rey, A. (2015). Mind the gap: Non-biological processes contributing to soil CO_2 efflux. *Global Change Biology*, *21*(5), 1752–1761. https://doi.org/10.1111/gcb.12821
Risk, D., Kellman, L., & Beltrami, H. (2008). A new method for in situ soil gas diffusivity measurement and applications in the monitoring of subsurface CO_2 production. *Journal of Geophysical Research*, *113*, G02018. https://doi.org/10.1029/2007JG000445
Rochette, P., Desjardins, R. L., & Pattey, E. (1991). Spatial and temporal variability of soil respiration in agricultural fields. *Canadian Journal of Soil Science*, *71*(2), 189–196. https://doi.org/10.4141/cjss91-018
Roland, M., Vicca, S., Bahn, M., Ladreiter-Knauss, T., Schmitt, M., & Janssens, I. A. (2015). Importance of nondiffusive transport for soil CO_2 efflux in a temperate mountain grassland. *Journal of Geophysical Research: Biogeosciences*, *120*, 502–512. https://doi.org/10.1002/2014JG002788
Ryan, E., Ogle, K., Kropp, H., Samuels-Crow, K. E., Carrillo, Y., & Pendall, E. (2018). Modelling soil CO_2 production and transport with dynamic source and diffusion terms: Testing the steady-state assumption using DETECT v1.0. *Geoscientific Model Development*. https://doi.org/10.5194/gmd-11-1-2018
Ryan, E. M., Ogle, K., Zelikova, T. J., LeCain, D. R., Williams, D. G., Morgan, J. A., & Pendall, E. (2015). Antecedent moisture and temperature conditions modulate the response of ecosystem respiration to elevated CO_2 and warming. *Global Change Biology*, *21*(7), 2588–2602. https://doi.org/10.1111/gcb.12910
Ryan, M. G., & Law, B. E. (2005). Interpreting, measuring, and modeling soil respiration. *Biogeochemistry*, *73*(1), 3–27. https://doi.org/10.1007/s10533-004-5167-7
Sala, O. E., Lauenroth, W. K., & Parton, W. J. (1992). Long-term soil water dynamics in the shortgrass steppe. *Ecology*, *73*(4), 1175–1181. https://doi.org/10.2307/1940667
Schlesinger, W., & Andrews, J. (2000). Soil respiration and the global carbon cycle. *Biogeochemistry*, *48*(1), 7–20. https://doi.org/10.1023/A:1006247623877
Sierra, C. A. (2012). Temperature sensitivity of organic matter decomposition in the Arrhenius equation: Some theoretical considerations. *Biogeochemistry*, *108*(1–3), 1–15. https://doi.org/10.1007/s10533-011-9596-9
Šimůnek, J., & Suarez, D. L. (1993). Modeling of carbon dioxide transport and production in soil 1. Model development. *Water Resources Research*, *29*(2), 487–497. https://doi.org/10.1029/92WR02225
Šimůnek, J., Van Genuchten, M., & Sejna, M. (2012). HYDRUS: Model use, calibration, and validation. *Transactions of the ASABE*, *38*(12), 63-1–63-12. https://doi.org/10.1029/2002WR001340; Bradford, S.A., Šimůnek, J., Bettehar, M., Van, http://g.m.th., Yates, S.R., Modeling colloid attachment, straining, and exclusion in saturated porous media (2003) Environ. Sci. Tech., 37 (10), pp. 2242–2250; Bradford, S.A., Bettehar, M., Šimůnek, J., Van Genuchten, M.Th., Straining and attachment of colloids in physically heterogeneous porous media (2004) Vadose Zone J., 3 (2), pp. 384–394; Brooks, R.H., Corey, A.T., (1964) Hydraulic Properties of Porous Media, Hydrology Paper
Šimůnek, J., van Genuchten, M. T., & Šejna, M. (2008). Development and applications of the HYDRUS and STANMOD software packages and related codes. *Vadose Zone Journal*, *7*(2), 587. https://doi.org/10.2136/vzj2007.0077
Stoy, P. C., Palmroth, S., Oishi, A. C., Siqueira, M. B. S., Juang, J. Y., Novick, K. A., et al. (2007). Are ecosystem carbon inputs and outputs coupled at short time scales? A case study from adjacent pine and hardwood forests using impulse-response analysis. *Plant, Cell and Environment*, *30*(6), 700–710. https://doi.org/10.1111/j.1365-3040.2007.01655.x
Takahashi, Y., Liang, N., Hirata, R., Machida, T., & Fujinuma, Y. (2008). Variability in carbon stable isotope ratio of heterotrophic respiration in a deciduous needle-leaf forest. *Journal of Geophysical Research*, *113*, G01022. https://doi.org/10.1029/2007JG000478.

Tang, J., & Baldocchi, D. D. (2005). Spatial-temporal variation in soil respiration in an oak-grass savanna ecosystem in California and its partitioning into autotrophic and heterotrophic components. *Biogeochemistry*, *73*(1), 183–207. https://doi.org/10.1007/s10533-004-5889-6

Tang, J., Baldocchi, D. D., Qi, Y., & Xu, L. (2003). Assessing soil CO_2 efflux using continuous measurements of CO_2 profiles in soils with small solid-state sensors. *Agricultural and Forest Meteorology*, *118*(3–4), 207–220. https://doi.org/10.1016/S0168-1923(03)00112-6

Tang, J., & Riley, W. J. (2014). Weaker soil carbon-climate feedbacks resulting from microbial and abiotic interactions. *Nature Climate Change*, *5*(1), 56–60. https://doi.org/10.1038/nclimate2438

Tian, H., Lu, C., Yang, J., Banger, K., Huntzinger, D. N., Schwalm, C. R., et al. (2015). Global patterns and controls of soil organic carbon dynamics as simulated by multiple terrestrial biosphere models: Current status and future directions. *Global Biogeochemical Cycles*, *29*, 775–792. https://doi.org/10.1002/2014GB005021

Todd-Brown, K. E. O., Hopkins, F. M., Kivlin, S. N., Talbot, J. M., & Allison, S. D. (2012). A framework for representing microbial decomposition in coupled climate models. *Biogeochemistry*, *109*(1–3), 19–33. https://doi.org/10.1007/s10533-011-9635-6

Todd-Brown, K. E. O., Randerson, J. T., Post, W. M., Hoffman, F. M., Tarnocai, C., Schuur, E. A. G., & Allison, S. D. (2013). Causes of variation in soil carbon simulations from CMIP5 Earth system models and comparison with observations. *Biogeosciences*, *10*(3), 1717–1736. https://doi.org/10.5194/bg-10-1717-2013

Torrence, C., & Compo, G. P. (1998). A practical guide to wavelet analysis. *Bulletin of the American Meteorological Society*, *79*(1), 61–78. https://doi.org/10.1175/1520-0477(1998)079%3C0061:APGTWA%3E2.0.CO;2

Vargas, R., Baldocchi, D. D., Allen, M. F., Bahn, M., Black, T. A., Collins, S. L., et al. (2010). Looking deeper into the soil: Biophysical controls and seasonal lags of soil CO_2 production and efflux. *Ecological Applications*, *20*(6), 1569–1582. https://doi.org/10.1890/09-0693.1

Vargas, R., Baldocchi, D. D., Bahn, M., Hanson, P. J., Hosman, K. P., Kulmala, L., et al. (2011). On the multi-temporal correlation between photosynthesis and soil CO_2 efflux: Reconciling lags and observations. *New Phytologist*, *191*(4), 1006–1017. https://doi.org/10.1111/j.1469-8137.2011.03771.x

Vargas, R., Detto, M., Baldocchi, D. D., & Allen, M. F. (2010). Multiscale analysis of temporal variability of soil CO_2 production as influenced by weather and vegetation. *Global Change Biology*, *16*(5), 1589–1605. https://doi.org/10.1111/j.1365-2486.2009.02111.x

Wang, X., Liu, L., Piao, S., Janssens, I. A., Tang, J., Liu, W., et al. (2014). Soil respiration under climate warming: Differential response of heterotrophic and autotrophic respiration. *Global Change Biology*, *20*(10), 3229–3237. https://doi.org/10.1111/gcb.12620

Xu, L., & Baldocchi, D. D. (2004). Seasonal variation in carbon dioxide exchange over a Mediterranean annual grassland in California. *Agricultural and Forest Meteorology*, *123*(1–2), 79–96. https://doi.org/10.1016/j.agrformet.2003.10.004

Zelikova, T. J., Blumenthal, D. M., Williams, D. G., Souza, L., LeCain, D. R., Morgan, J., & Pendall, E. (2014). Long-term exposure to elevated CO_2 enhances plant community stability by suppressing dominant plant species in a mixed-grass prairie. *Proceedings of the National Academy of Sciences of the United States of America*, *111*(43), 15,456–15,461. https://doi.org/10.1073/pnas.1414659111

Zelikova, T. J., Williams, D., Hoenigman, R., Blumenthal, D. M., Morgan, J. A., & Pendall, E. (2015). Seasonality of soil moisture mediates responses of ecosystem phenology to elevated CO_2 and warming in a semi-arid grassland. *Journal of Ecology*, *103*(5), 1119–1130. https://doi.org/10.1111/1365-2745.12440

Zhang, Q., Katul, G. G., Oren, R., Daly, E., Manzoni, S., & Yang, D. (2015). The hysteresis response of soil CO_2 concentration and soil respiration to soil temperature. *Journal of Geophysical Research: Biogeosciences*, *120*, 1605–1618. https://doi.org/10.1002/2015JG003047

Zobitz, J. M., Moore, D. J. P., Sacks, W. J., Monson, R. K., Bowling, D. R., & Schimel, D. S. (2008). Integration of process-based soil respiration models with whole-ecosystem CO_2 measurements. *Ecosystems*, *11*(2), 250–269. https://doi.org/10.1007/s10021-007-9120-1